Muons under extreme conductions: Pressure

Rustem Khasanov, PSI, Switzerland
International Advanced School on Muon Spectroscopy, 15-22 August 2019

Outline

- Principles of μSR under pressure experiments:
  - beam-lines
  - Spectrometers
  - Pressure cells
- "Decay" beam-lines
- μE1 decay beam-line at PSI
- General Purpose Decay (GPD) spectrometer
- Pressure cell construction(s)
- Pressure measurements

- Scientific examples
  - Interplay between superconductivity and magnetism in CrAs

μSR under pressure: Basic principles

Principle of μSR under pressure experiments

Muon momentum tuning

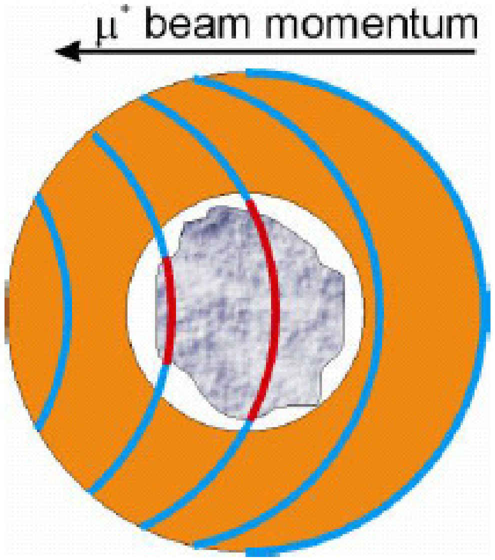

Beam-width tuning

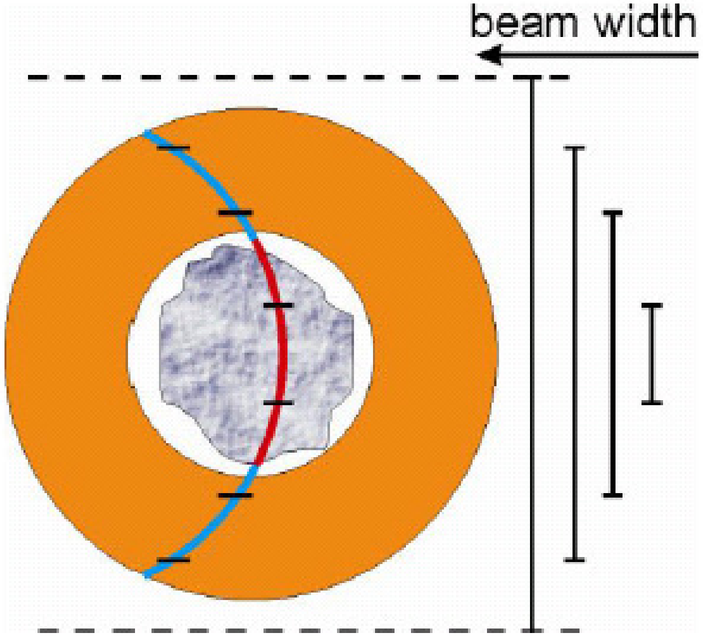

μSR under pressure

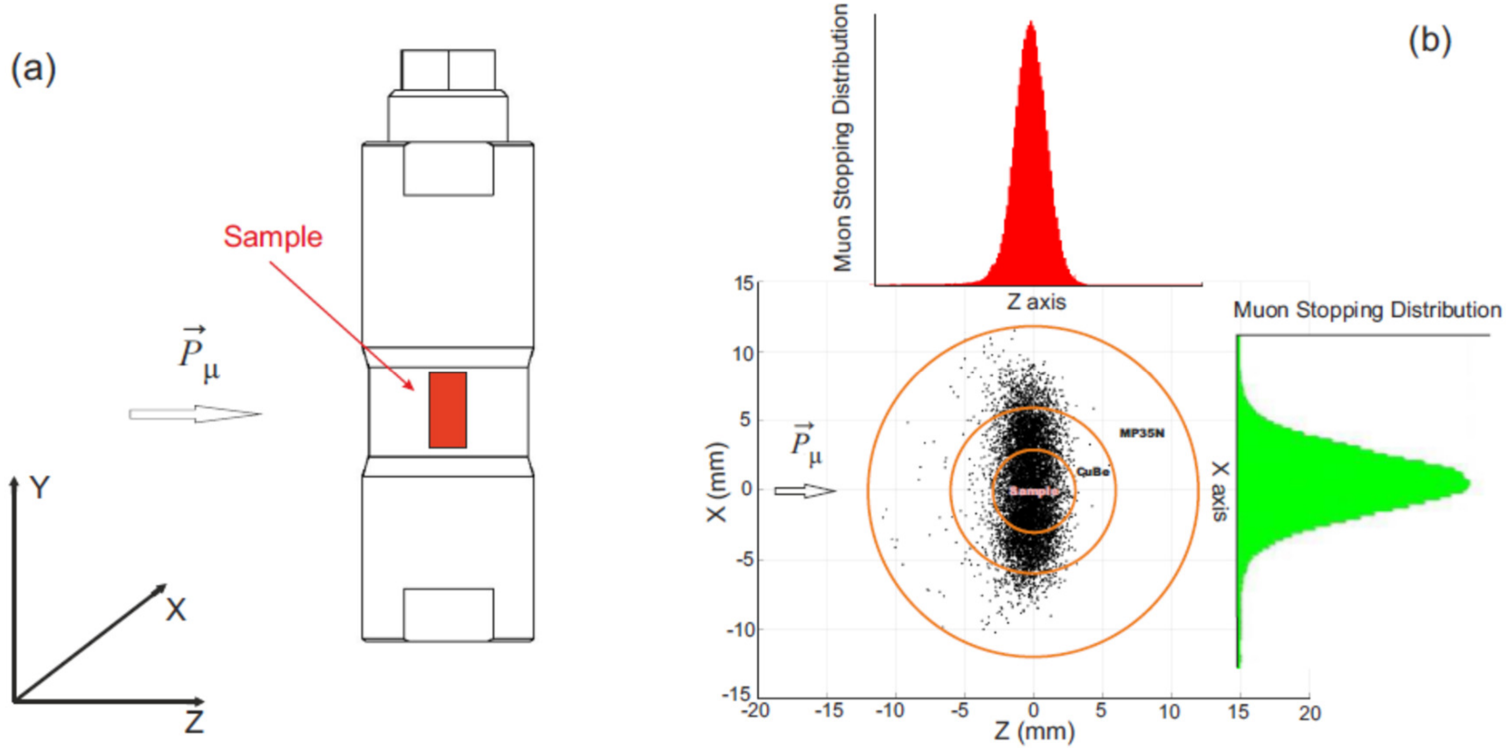

The schematic view of the pressure cell (black contour) with the sample (red rectangular). Muons are implanted along the vector P. (b) The cross sectional view (X-Z plane) of the double-wall pressure cell. The colored areas represent the muon stopping distributions in parallel (red) and perpendicular (green) direction to the muon beam. The energy of implanted muons is 44 MeV. The simulations were made by using TRIM.SP package. The simulations reveal that approximately 37% of all the muons stop within the sample, 43% within the inner and 10% within the outer cylinder.

PAUL SCHERRER INSTITUT

μSR under pressure: muon momentum and beam-lines

Muon Implantation Depth

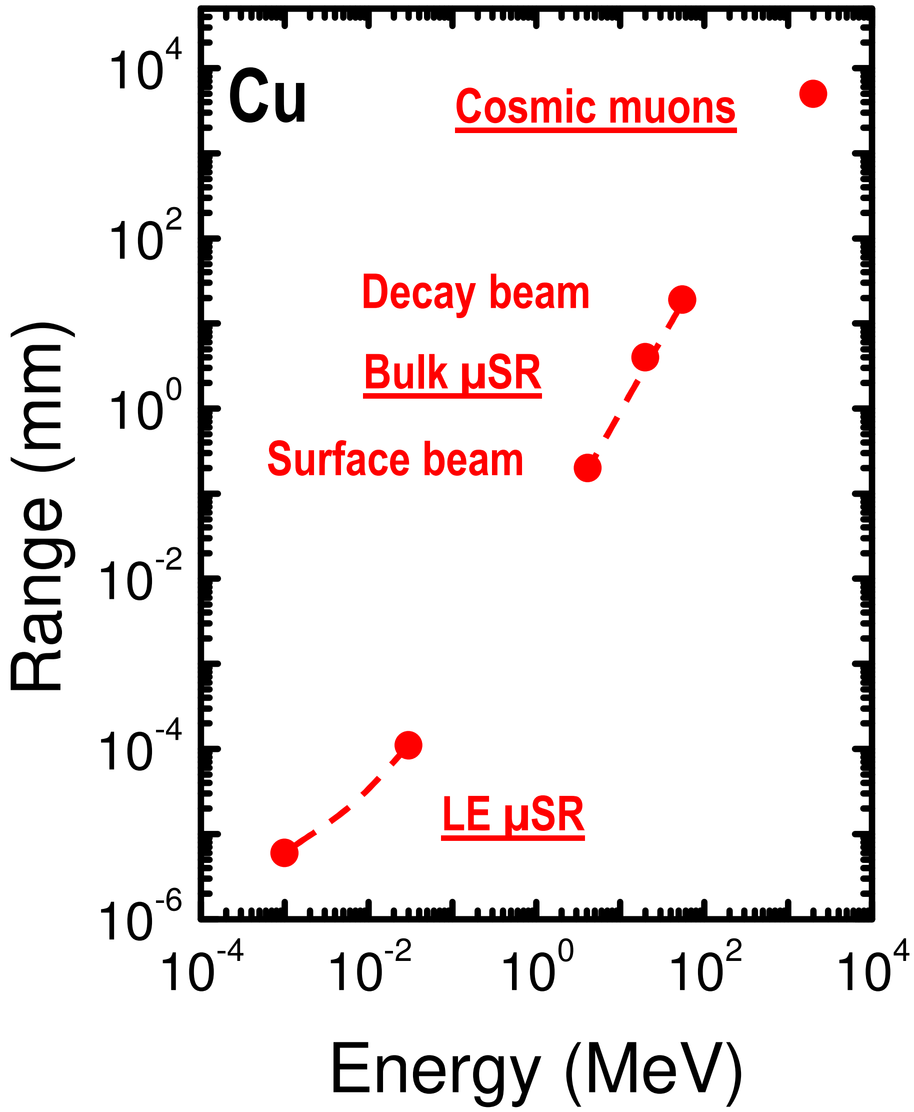

In order to perform muon experiments under pressure one needs to use the so-called 'decay' beam-lines

Decay muon beam-line

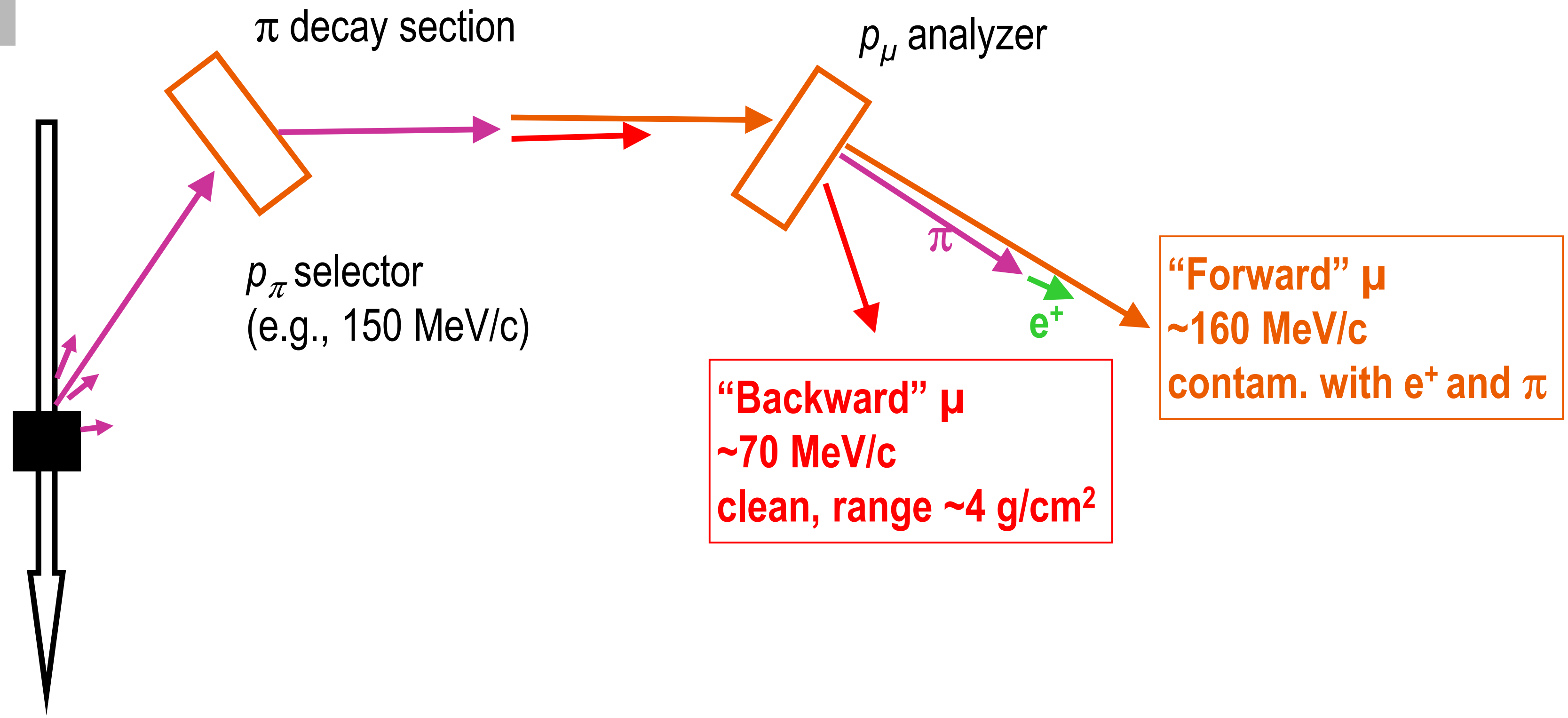

μE1 beam-line at PSI

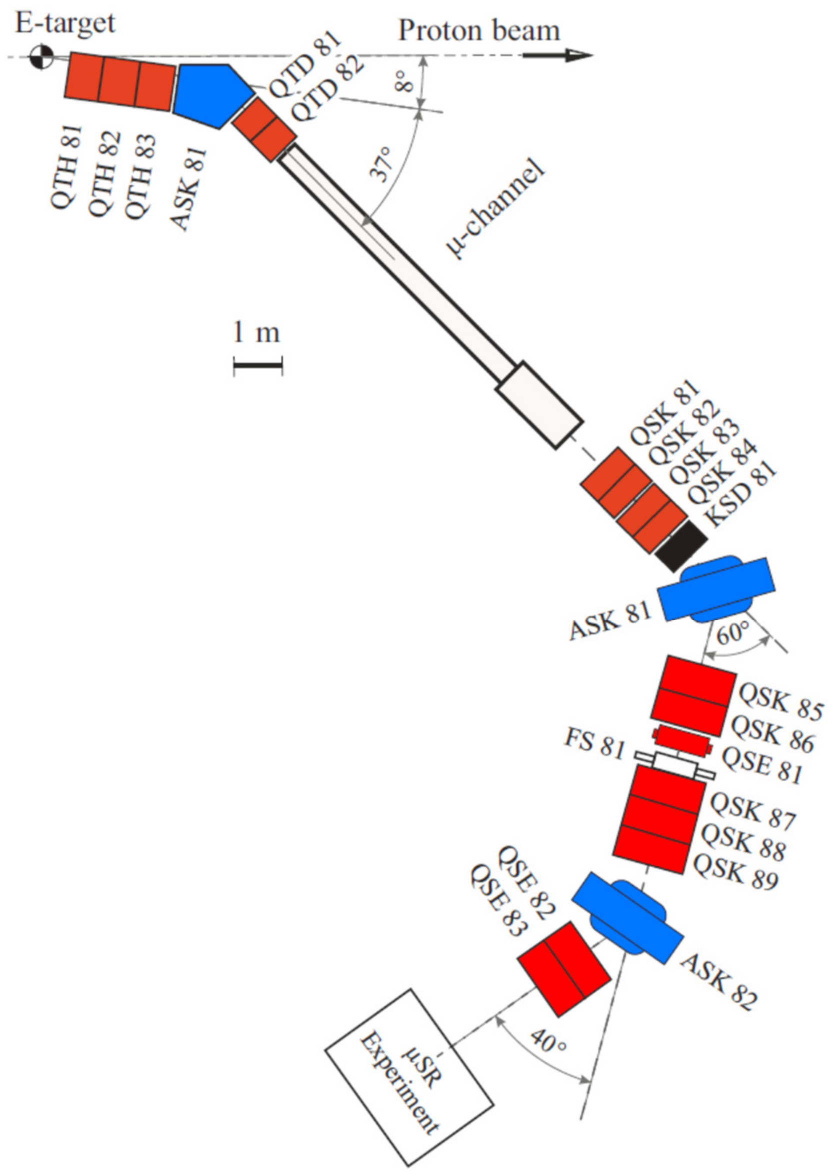

Momentum acceptance (FWHM)	3%
Pion momentum range [MeV/c]	200--125
Muon momentum range [MeV/c]	125– 60
Rate of positive muon [$mA^{-1}s^{-1}$]	6e7--3e7
Spot size (FWHM)	39 X 28 mm

µEl Beam-spot

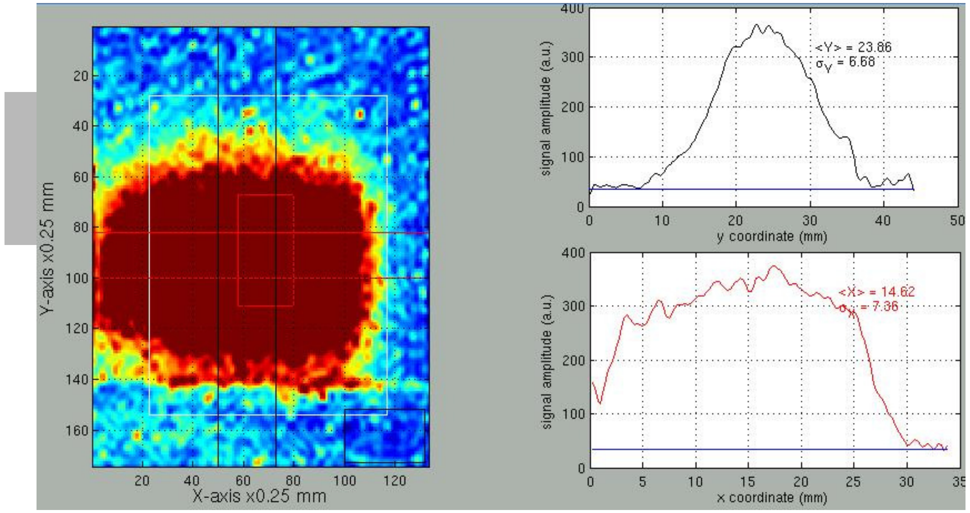

Direct beam. Beam setting p107apr09. Muon momentum 109 MeV/c

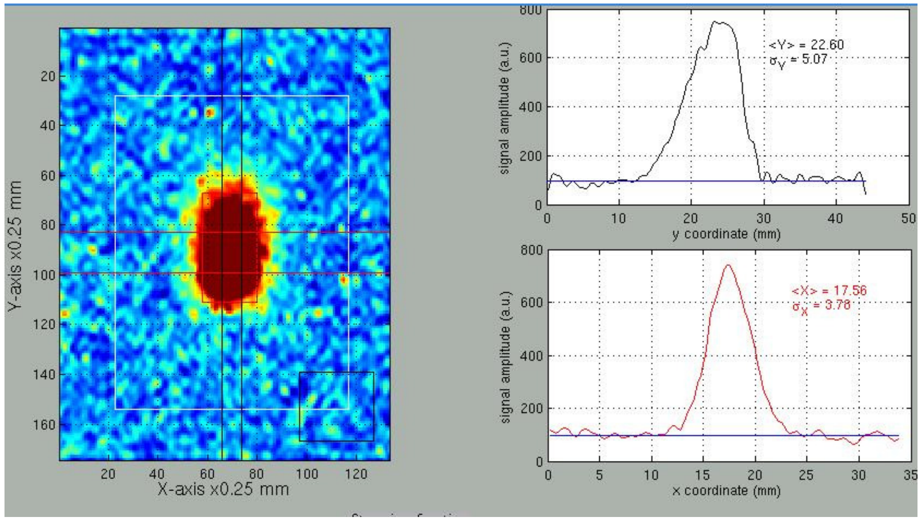

Collimated beam. Beam setting p107apr09. Muon momentum 109 MeV/c

μSR under pressure: GPD spectrometer

Construction of the detector block

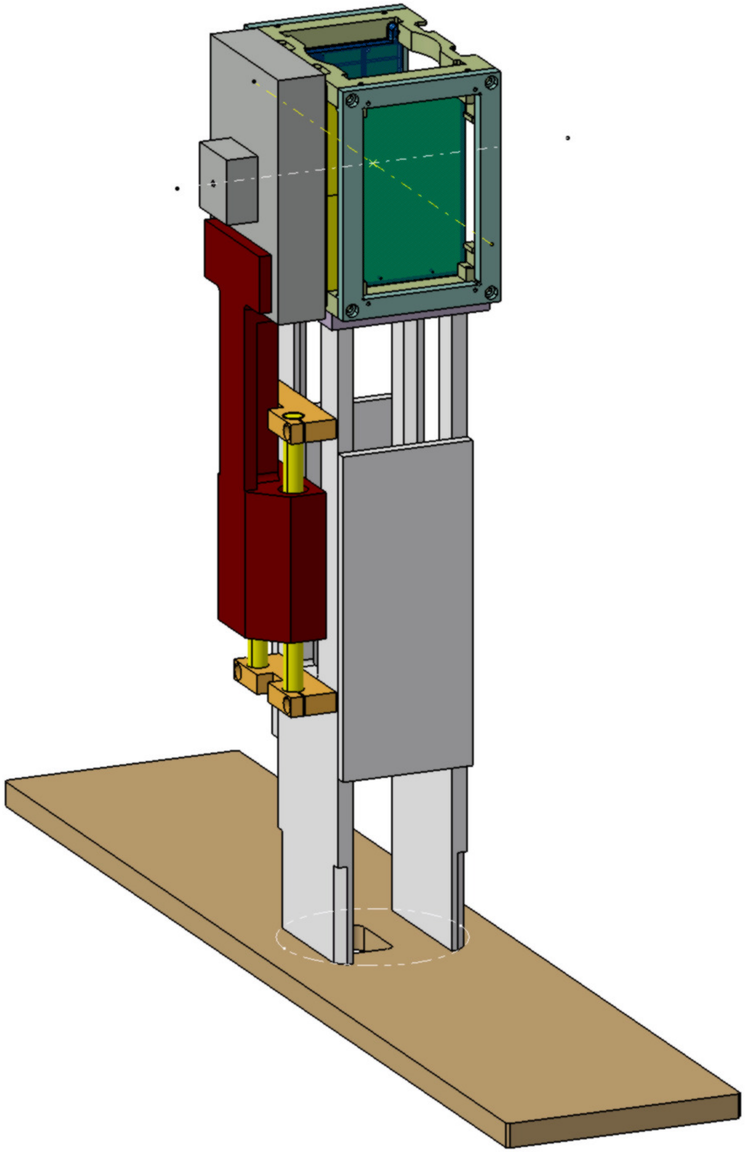

Vertical setup

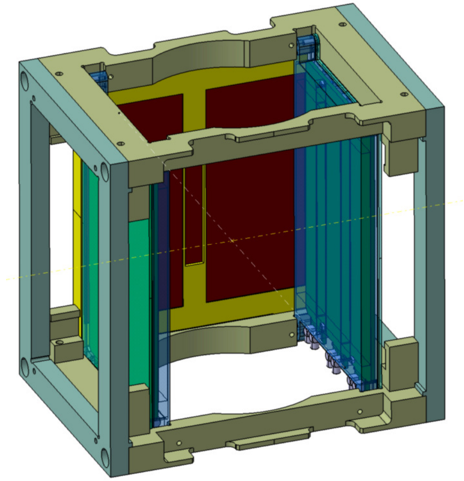

Horizontal setup

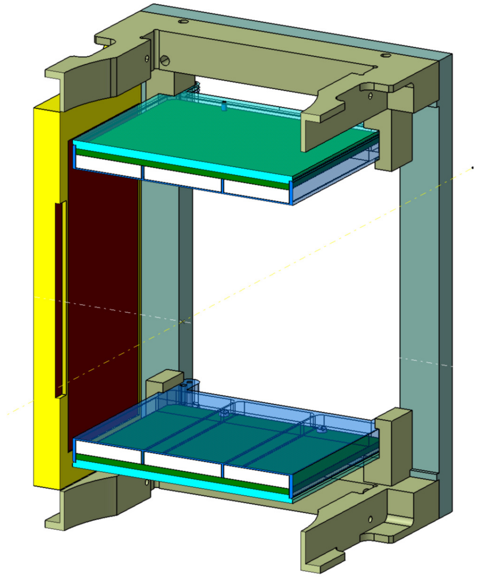

GPD instrument with the detectors

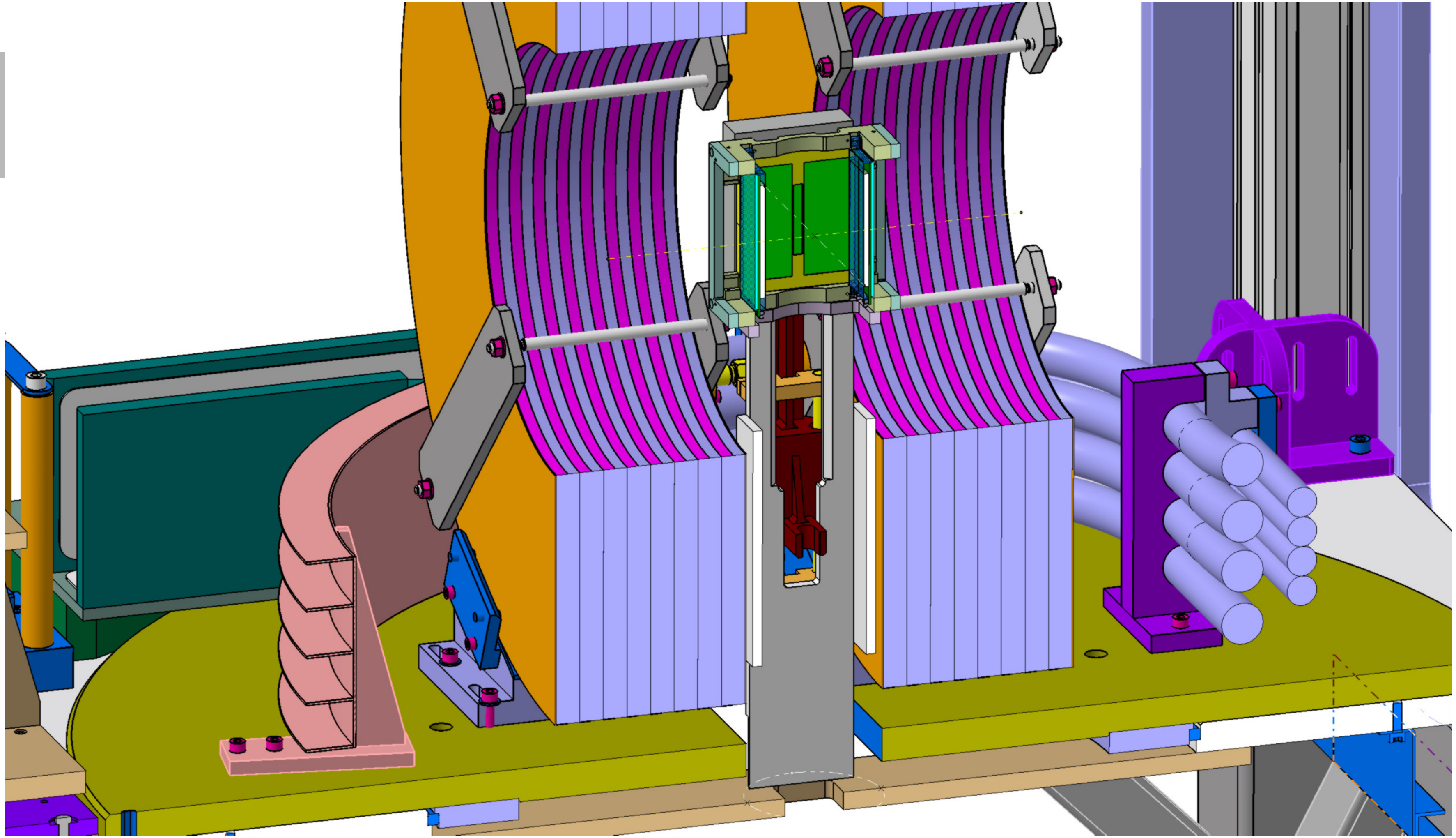

GPD instrument and cryostats

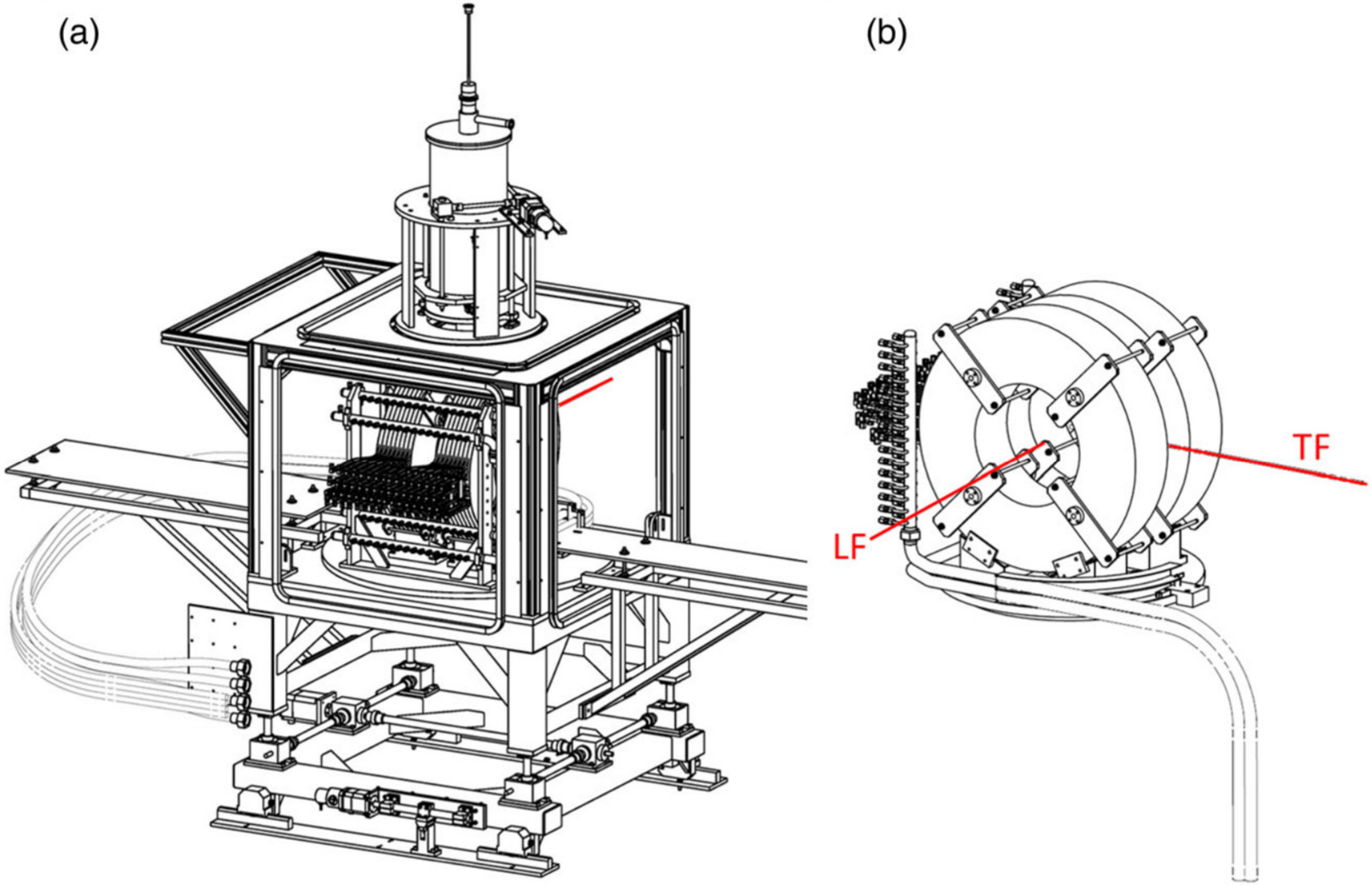

Sample cryostats available at the GPD instrument.

3He Sorption pumped	Oxford	0.24−325 K	Yes
4He gas flow	Janis	2.5−300 K	Yes
Closed Cycle Refr.	Home made	10−300 K	No
N_2 gas flow	Home made	80−500 K	No

Type of the pressure cell selection

μSR experiments under pressure – cell type selection

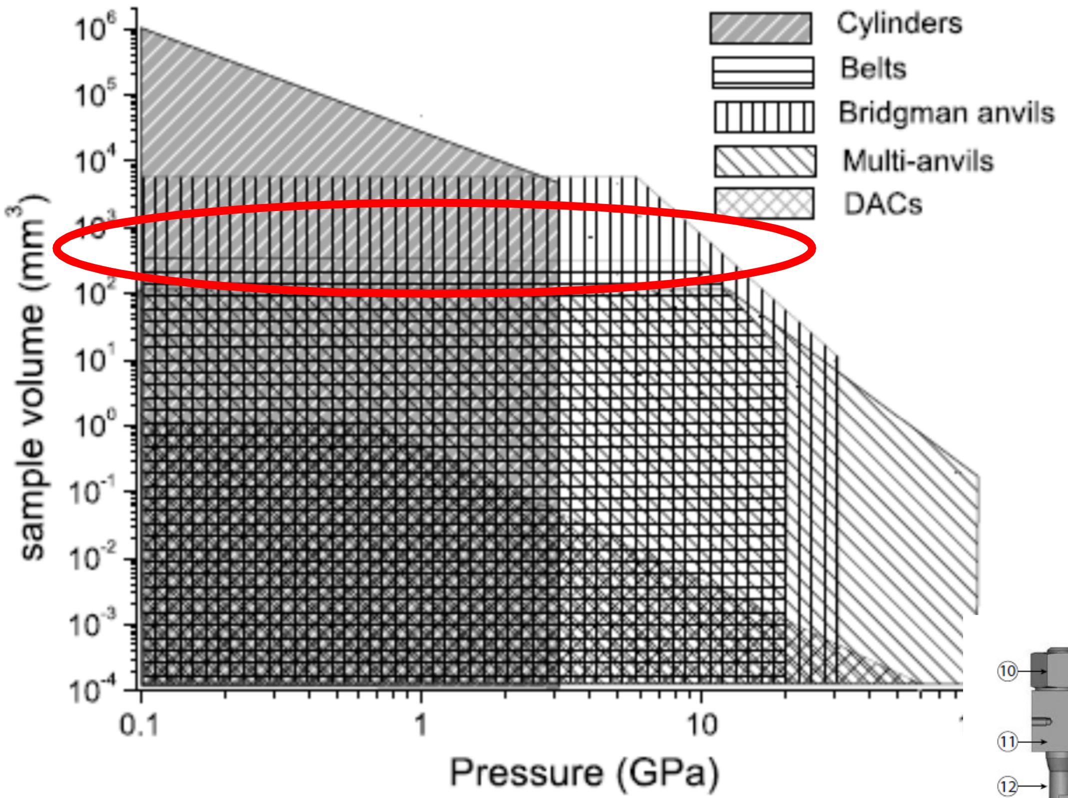

S. Klotz, Techniques in High Pressure Neutron Scattering

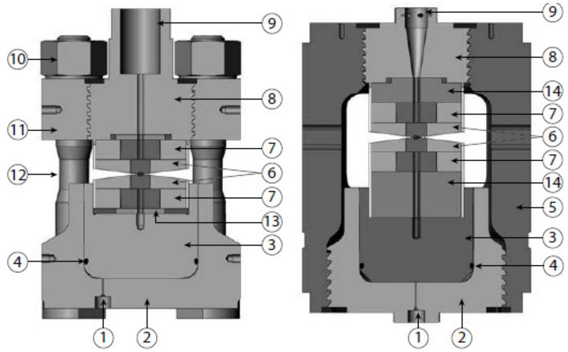

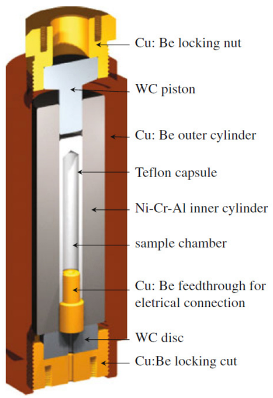

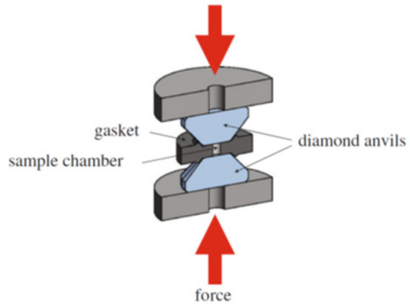

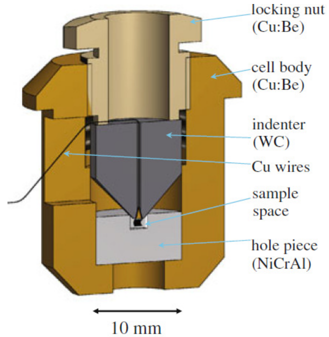

Contradicting criteria

- The pressure cell need to be small enough to fit inside the detector block
  - The pressure cell need to carry at least few hundred mm^3 sample
    - The pressure cell need to carry the highest possible pressure

↓

Only the piston-cylinder type of cell could satisfy them

The highest pressure is limited by ~2.5 GPa

PSI pressure cells

- 1980. Clamp cell. p_{max}= 0.7 Gpa / oil. Fe and Ni. [Butz et al., Phys. Lett. A 75, 321, 1980]
- 1986. Clamp cell. p_{max} = 1.4 Gpa / Helium. [Butz et al., Hyp. Int, 32, 881, 1986]
- 2001. Clamp cell. p_{max} = 0.9-1.4 Gpa / Liquid [Andreica, PhD thesis, ETHZ, 2001]
- 2009. Double-wall clamp cells. p_{max} = 2.8 Gpa / Liquid [Khasanov et al., High Pr. Res. 36, 140, 2016]

ISIS pressure cells

- 2009. Clamp cell. p_{max} = 0.6 Gpa / Helium [Watanabe et al., Physica B, 404, 993, 2009]

TRIUMF

- 2008. Clamp cell. p_{max} = 2.3 Gpa / Liquid [Goko, private communication]

PAUL SCHERRER INSTITUT

Pressure cell: design selection

Single and Double wall pressure cell construction

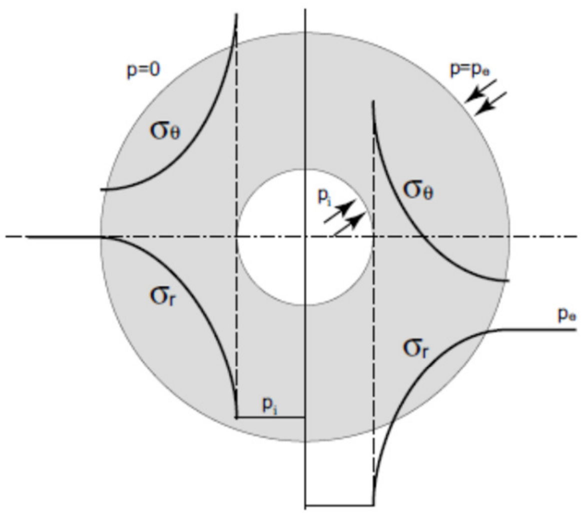

FIGURE 1.2
Stress distribution in a monobloc cylinder under two different conditions. Left: Internal pressure $p = p_i$ and external pressure $p = 0$. Right: Internal pressure $p = p_i$ and external pressure $p = p_e$.

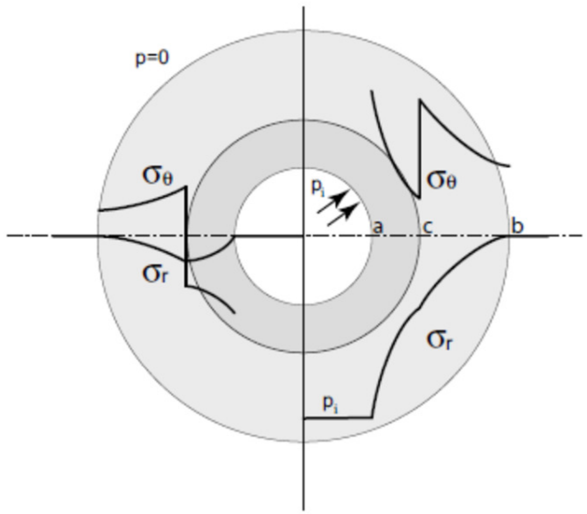

FIGURE 1.3
Stress distribution in a fretted (compound) cylinder. The left half shows the situation in the unloaded state (p_i=p_e=0), the right half under internal load.

S. Klotz, Techniques in High Pressure Neutron Scattering

Three wall double wall and single wall cells

Single wall cell | Double wall cell | Three wall cell

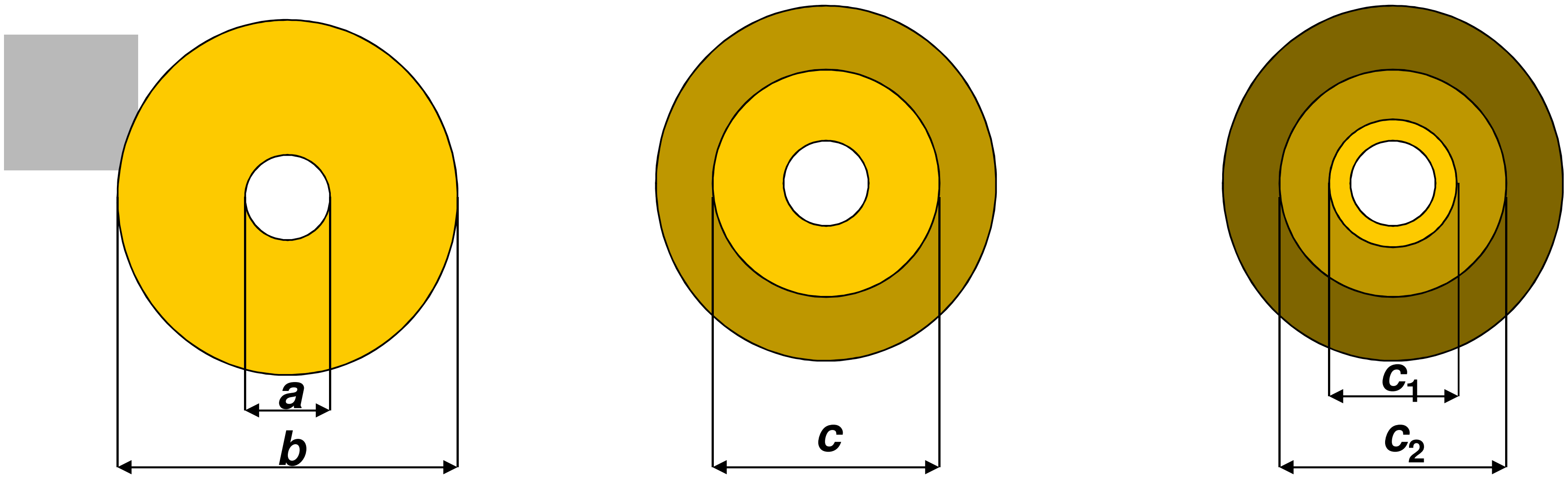

$$p_{max} \propto \frac{1}{2} - \frac{a^2}{2\,b^2}$$

$$p_{max} \propto 1 - \frac{a^2}{2\,c^2} - \frac{c^2}{2\,b^2}$$

$$p_{max} \propto \frac{3}{2} - \frac{a^2}{2\,c_1^{\,2}} - \frac{c_1^{\,2}}{2\,c_2^{\,2}} - \frac{c_2^{\,2}}{2\,b^2}$$

For ***a***=6 mm and ***b***=24 mm, $p_{max}^{\,s}$ / $p_{max}^{\,d}$ / $p_{max}^{\,t}$ = 1 / 2 / 2.4

Pressure cell: material selection

Construction material

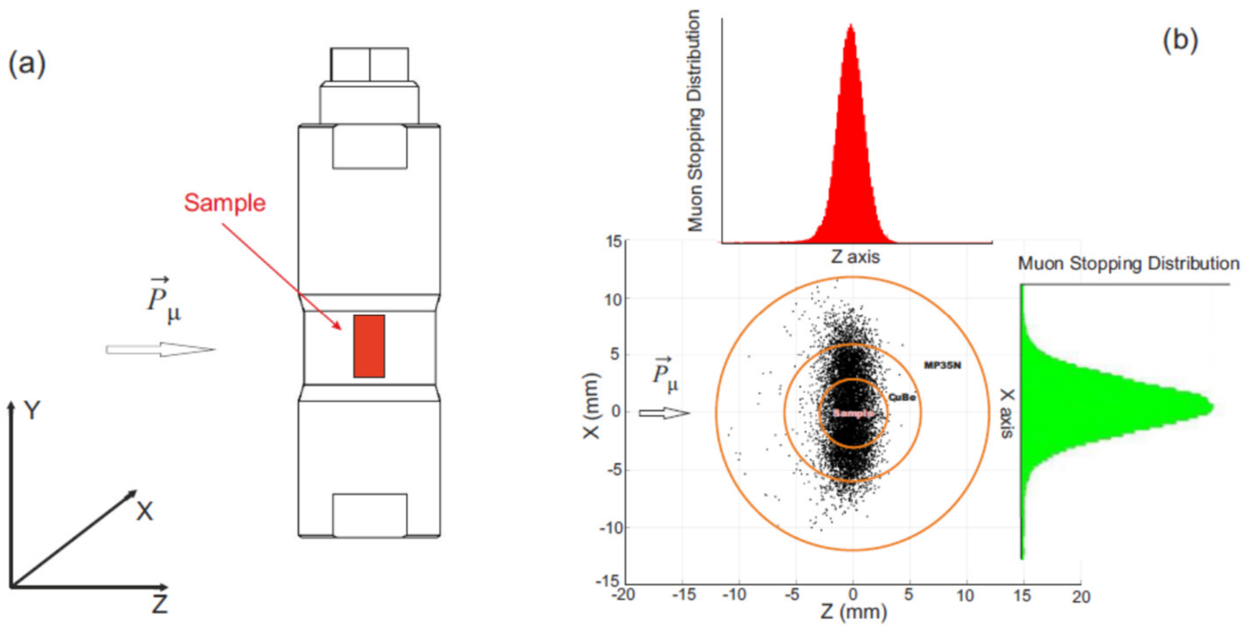

- Strong enough to hold the pressure
- Should not have "strong" μSR response
- Should have temperature independent responce

Construction material suitable for μSR

Nonmagnetic Alloys

	CuBe	$TiAl_6V_4$	NiCrAl	MP35N
Yield strength	1.1 Gpa (300 K)	1.05 Gpa (300 K)	2.06 Gpa (300 K)	2.15 GPa (300 K)
Young modulus	131 GPa (300 K)	97 Gpa (300 K)	190 Gpa (300 K)	215 Gpa (300 K)

Sintered materials

	WC	cBN	SiC	ZrO_2-Y_2O_3	Al_2O_3-ZrO_2	Si_3N_4
Compressive strength	5.0-11.0 Gpa	2.9 GPa	7.6-8.3 GPa	2.20 GPa	4.7 GPa	5.1-5.5 GPa
Young modulus	600-670 GPa		918 GPa	210 Gpa	357 GPa	241 GPa

Pressure cell: design and construction

Construction

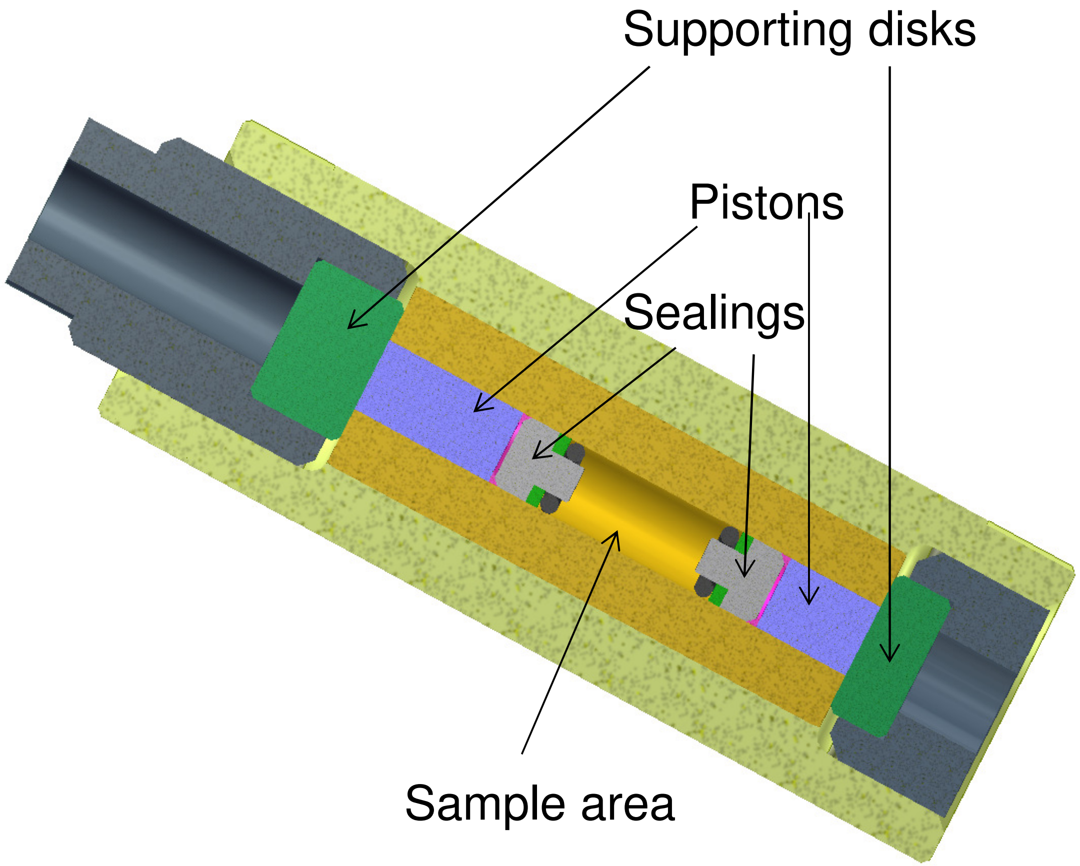

Material: MP35N (Ni 35%, Co 35%, Cr20%, Mo 10%)

Sample area: ø 6mm, height 12mm.

Muon stopping fraction: ~50-55%

Sealing

Modified Bridgman sealing

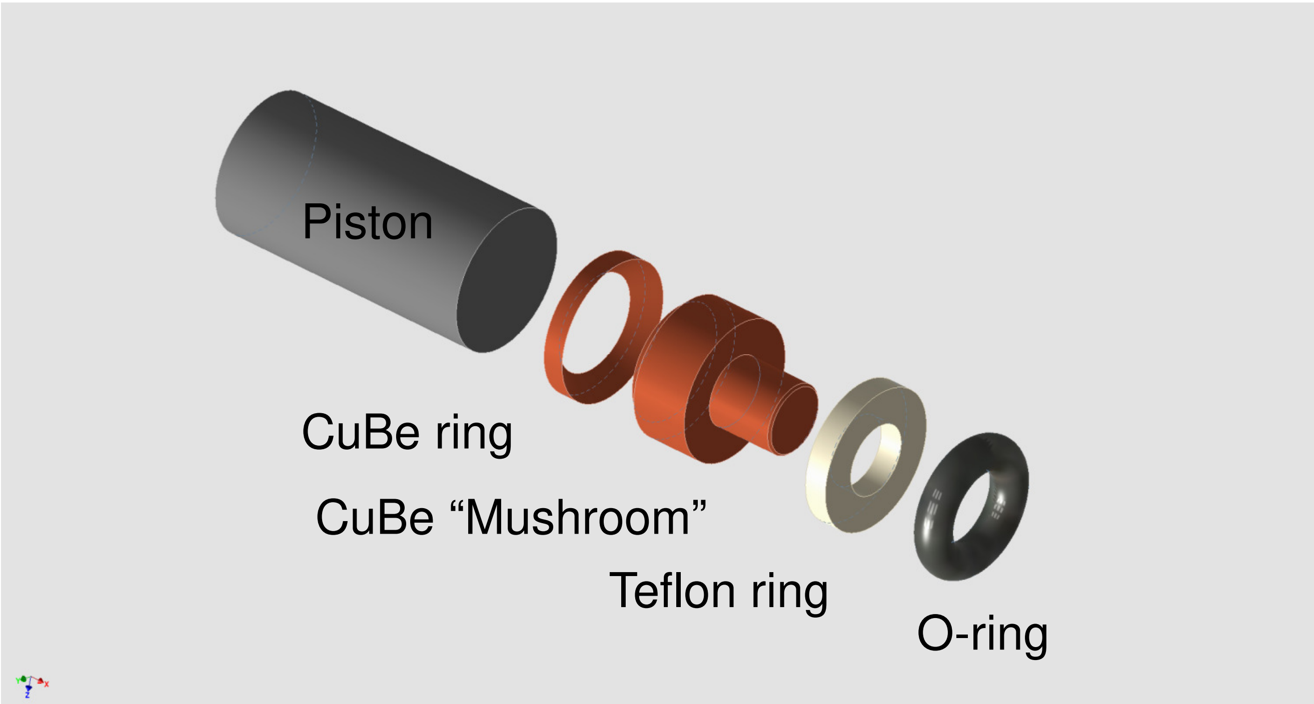

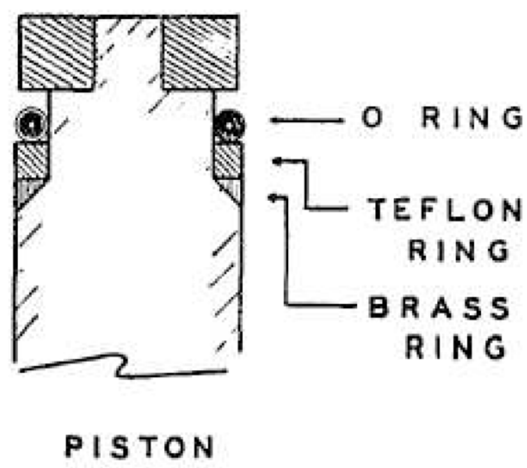

D. S. Hughes, W. W. Robertson, J. Opt. Soc. Am. **46,** 557 (1956)

Finite-Element analysis [CuBe/MP35N cell]

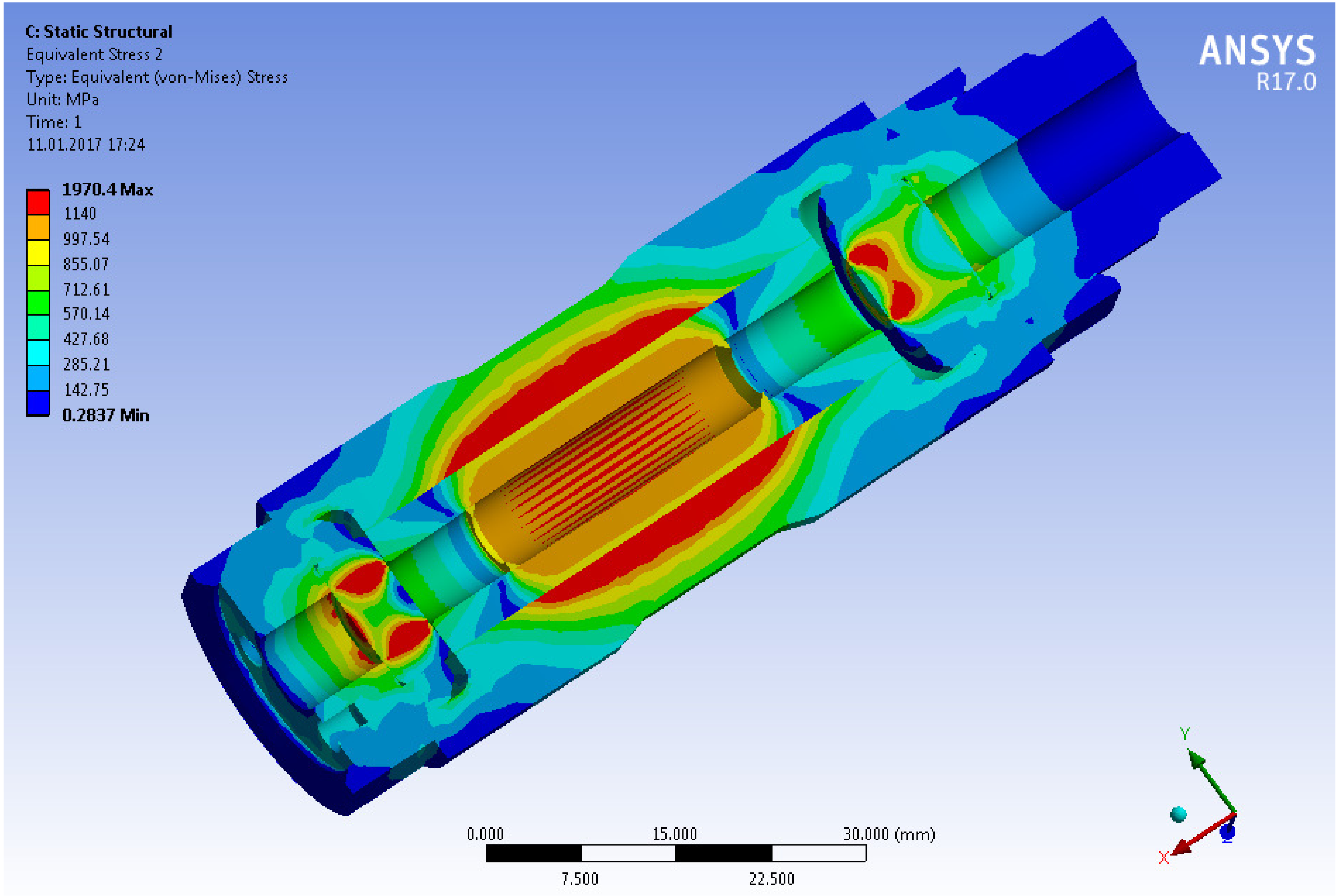

CuBe/MP35N frettage

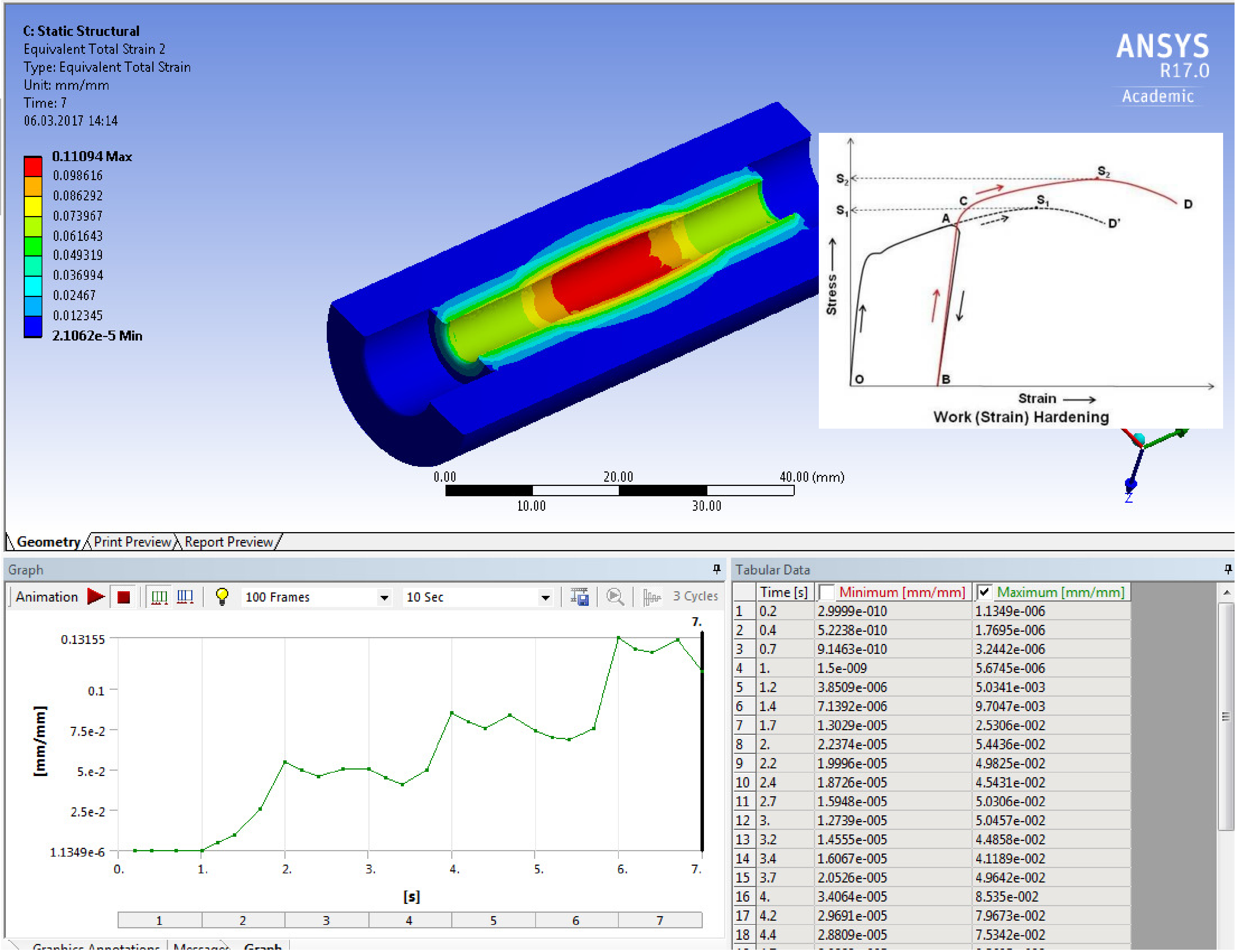

	Time [s]	Minimum [mm/mm]	Maximum [mm/mm]
1	0.2	2.9999e-010	1.1349e-006
2	0.4	5.2238e-010	1.7695e-006
3	0.7	9.1463e-010	3.2442e-006
4	1.	1.5e-009	5.6745e-006
5	1.2	3.8509e-006	5.0341e-003
6	1.4	7.1392e-006	9.7047e-003
7	1.7	1.3029e-005	2.5306e-002
8	2.	2.2374e-005	5.4436e-002
9	2.2	1.9996e-005	4.9825e-002
10	2.4	1.8726e-005	4.5431e-002
11	2.7	1.5948e-005	5.0306e-002
12	3.	1.2739e-005	5.0457e-002
13	3.2	1.4555e-005	4.4858e-002
14	3.4	1.6067e-005	4.1189e-002
15	3.7	2.0526e-005	4.9642e-002
16	4.	3.4064e-005	8.535e-002
17	4.2	2.9691e-005	7.9673e-002
18	4.4	2.8809e-005	7.5342e-002

Pressure determination

Pressure determination

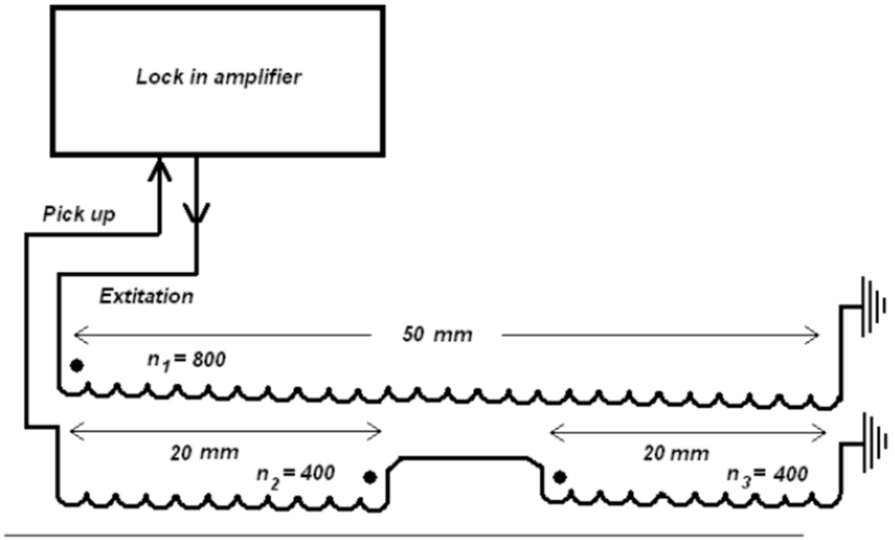

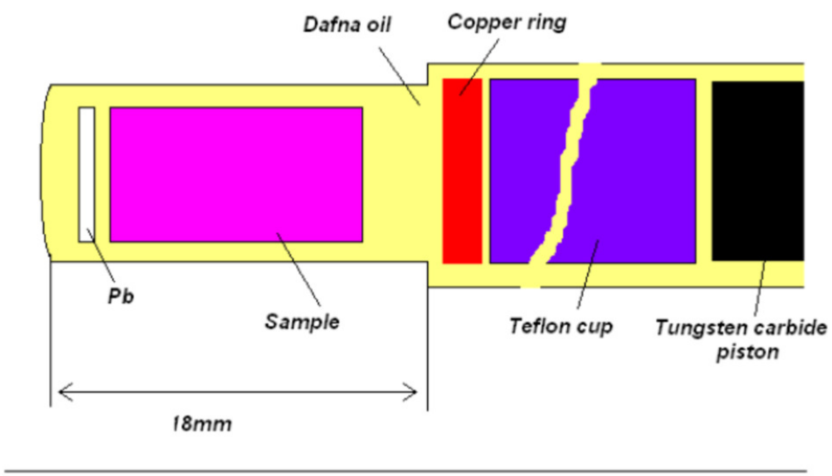

Mechatronische Mikropräzisions-Systeme

PAUL SCHERRER INSTITUT

Strain devices for μSR

Strain cell

Artem Nikitin

Matthias Elender

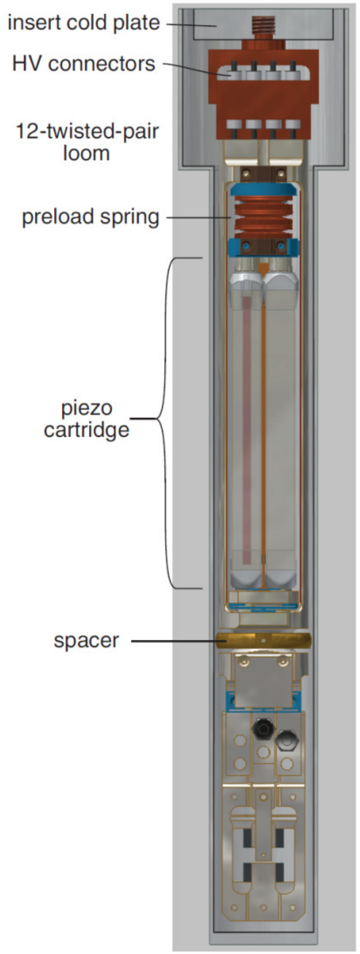

Hans-Henning Klauss
Rajib Sarkar

Vadim Grinenko

Shreenanda Ghosh

MAX-PLANCK-INSTITUT
FÜR CHEMISCHE PHYSIK FESTER STOFFE

Clifford Hicks

Working principle: compressive strain

- the cell is preloaded with force on the spring of 1000 N
- post 1 is epoxied to the cell frame, but not to the pass-thru plate, pass-thru plate can slide over the post 1
- **apply - 500 N on the piezo 1**
- the piezo 1 shrinks and moves the bridge downwards
- the spring expands

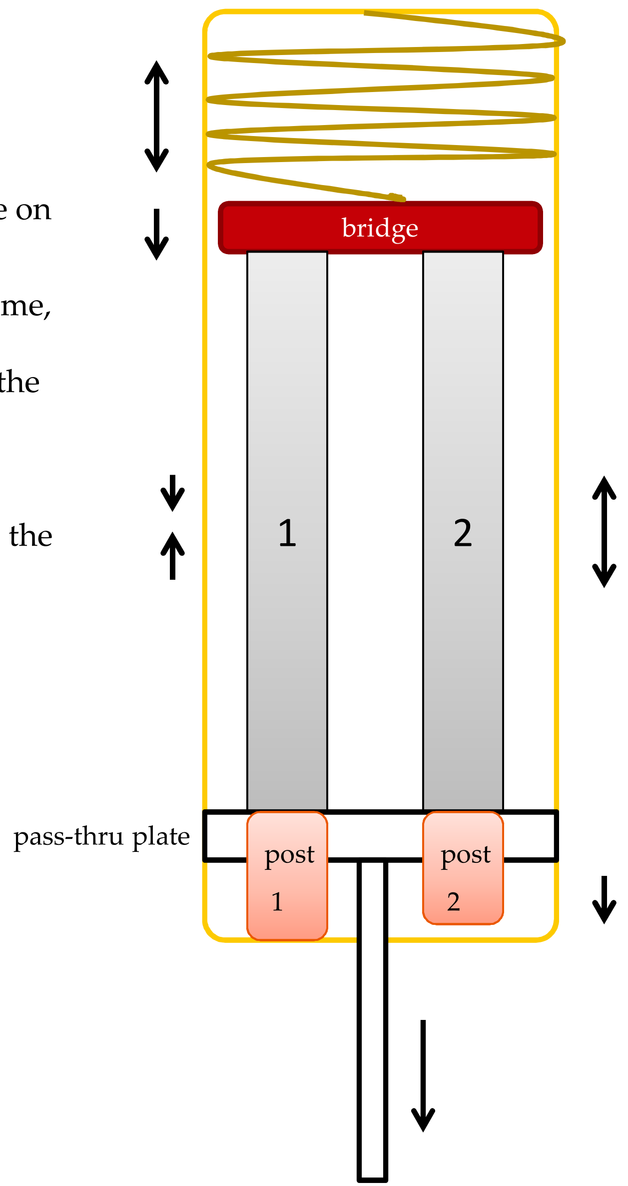

- **apply + 500 N on the piezo 2**
- the piezo 2 expands
- the piezo moves the post downwards
- the post 2 is epoxied to the pass-thru plate
- pass-thru plate moves downwards with force of + 500 N
- +500 N applies to the sample

PAUL SCHERRER INSTITUT

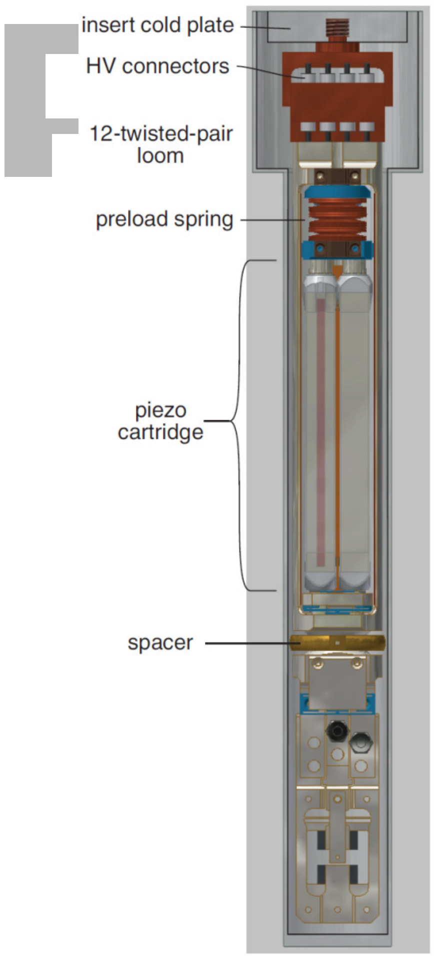

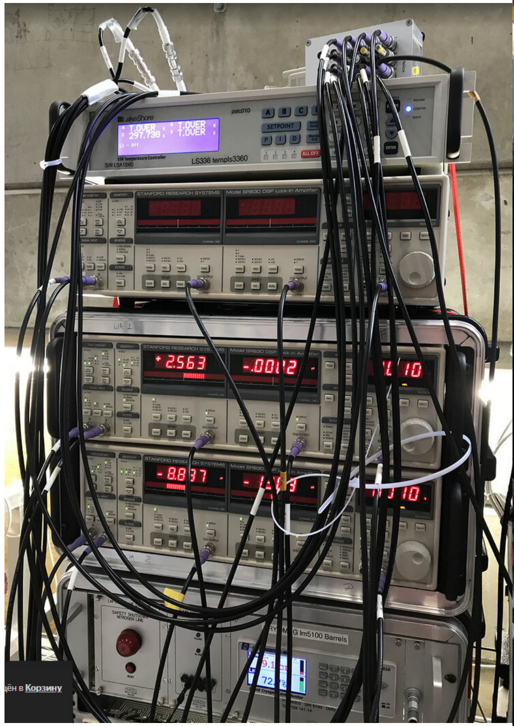

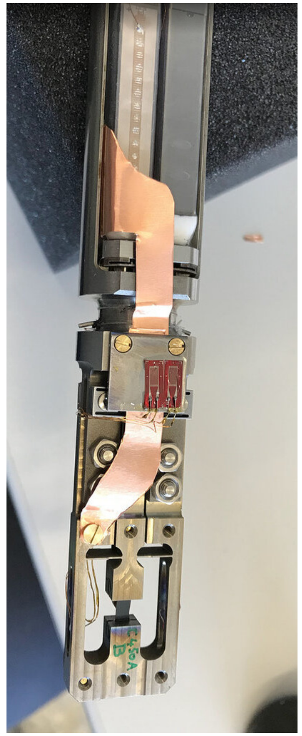

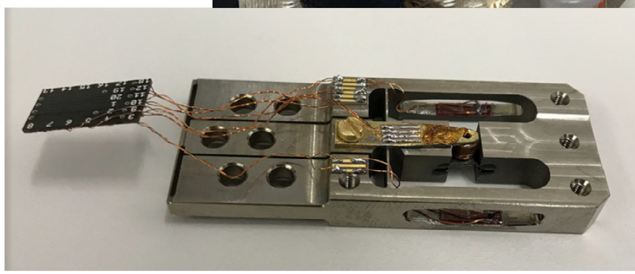

Lowest T = 0.7 K in ^{3}He cryostat

PAUL SCHERRER INSTITUT

Sr_2RuO_4

ZF relaxation rate (left)

AC susceptibility (right)

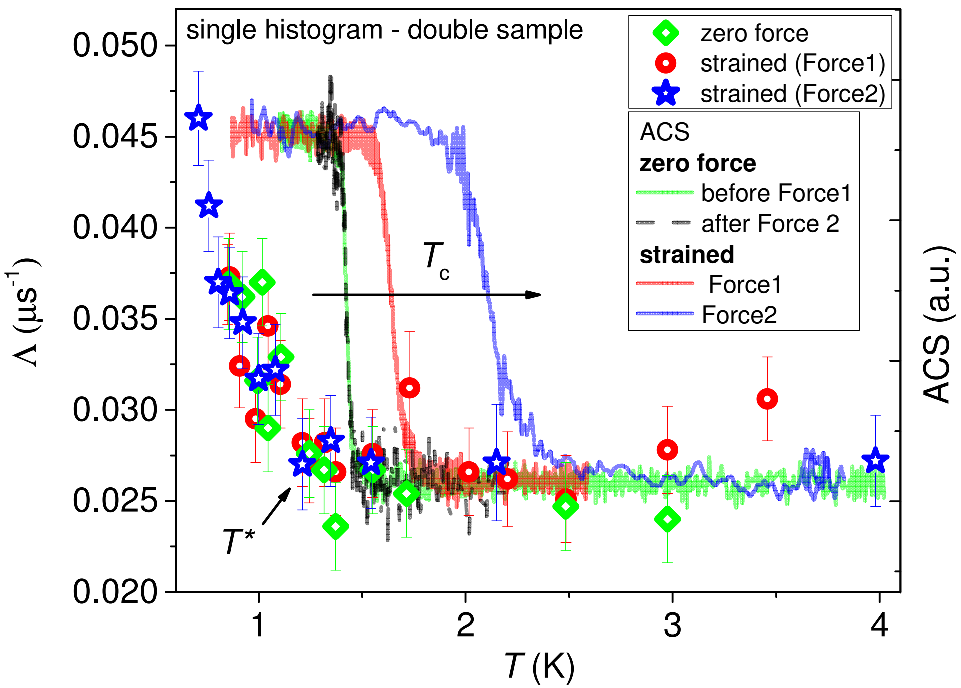

$CsFeCl_3$

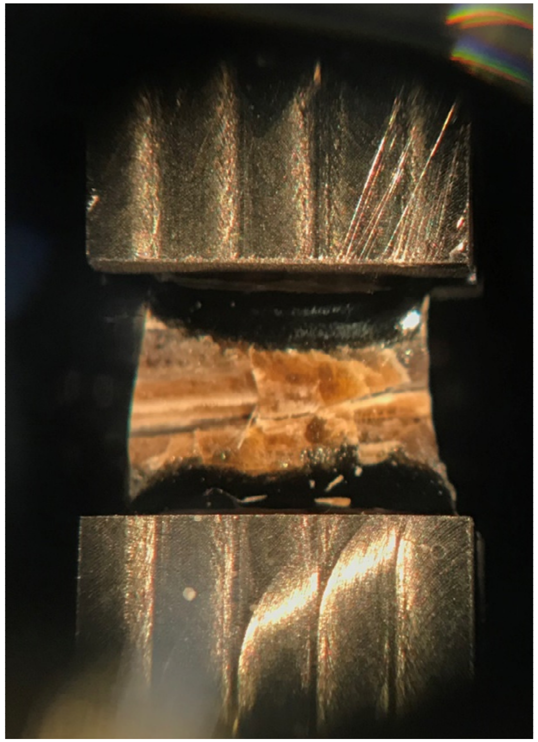

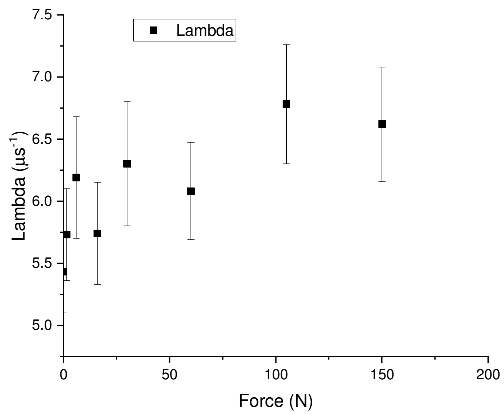

Future developments

Three wall double wall and single wall cells

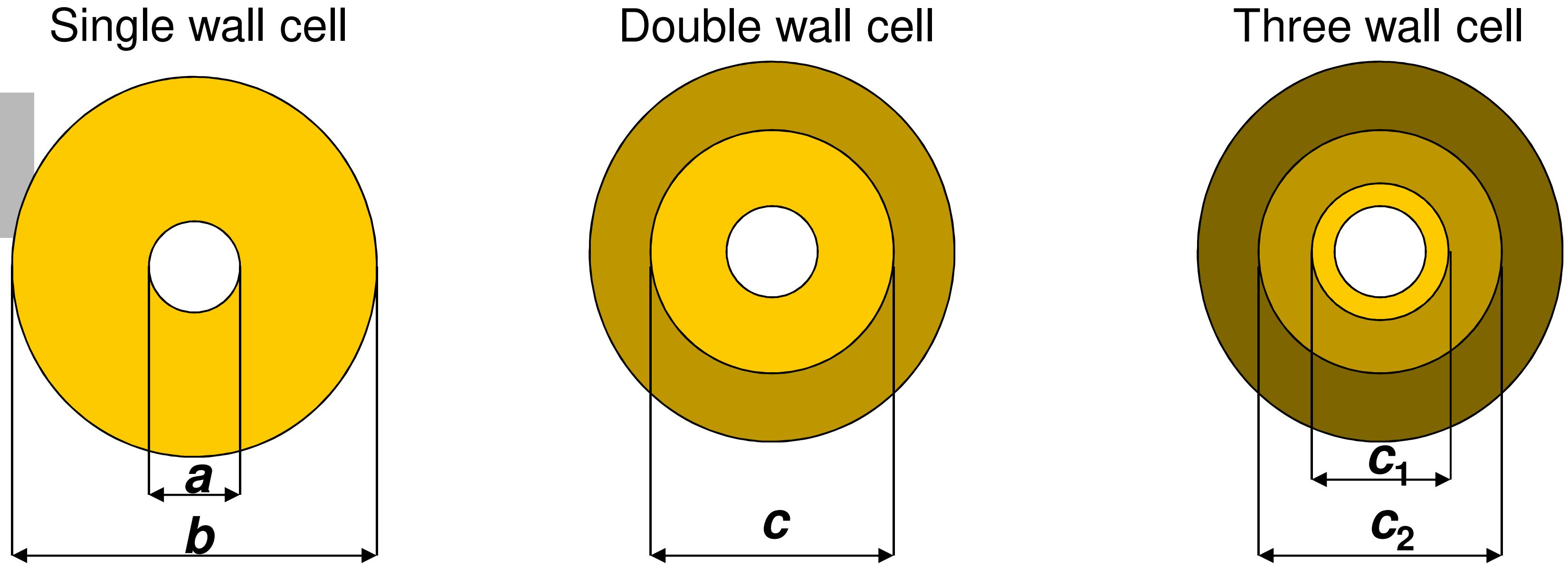

$$p_{max} \propto \frac{1}{2} - \frac{a^2}{2\,b^2}$$

$$p_{max} \propto 1 - \frac{a^2}{2\,c^2} - \frac{c^2}{2\,b^2}$$

$$p_{max} \propto \frac{3}{2} - \frac{a^2}{2\,c_1^2} - \frac{c_1^2}{2\,c_2^2} - \frac{c_2^2}{2\,b^2}$$

For ***a***=6 mm and ***b***=24 mm, p_{max}^{s} / p_{max}^{d} / p_{max}^{t} = 1 / 2 / 2.4

McWhan pressure cell

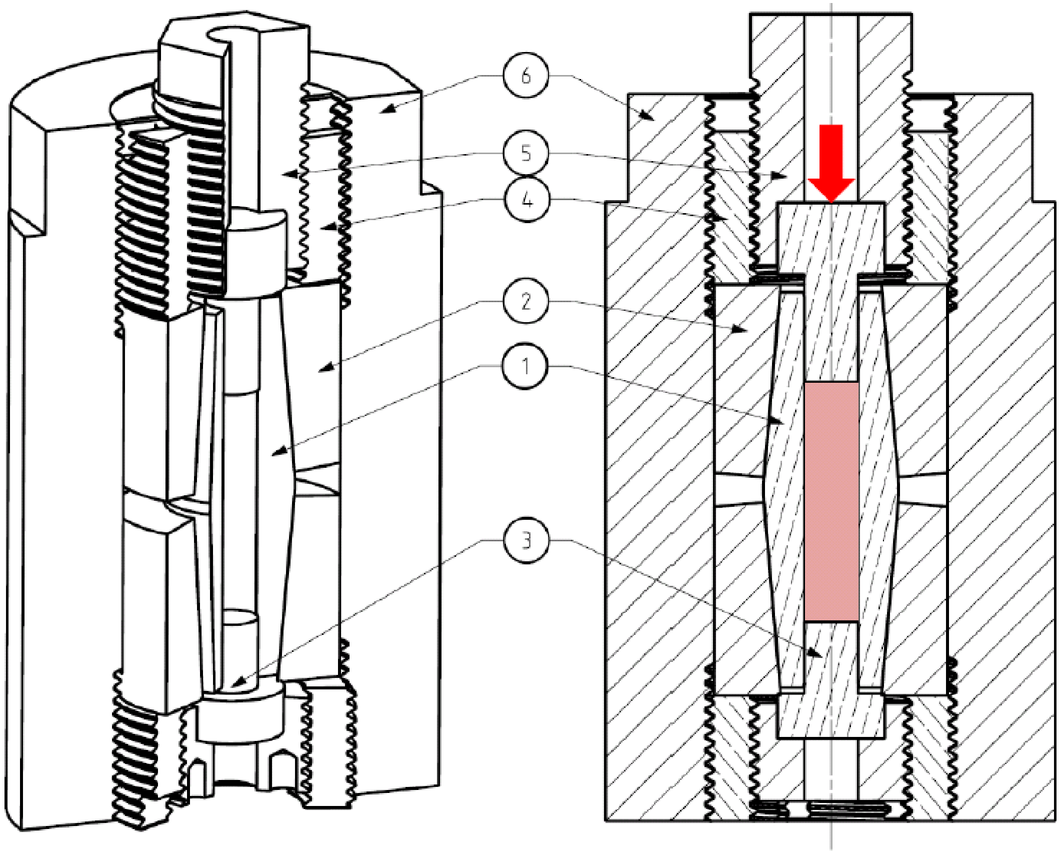

Components:
(1) bicone,
(2) compression pad,
(3) piston,
(4) outside locking pad,
(5) inside locking pad,
(6) Body

Materials:

- (1), (3): tungsten carbide
- (2), (5), (6): MP35N
- (4): copper beryllium

McWhan pressure cell

Anvil-type pressure cell

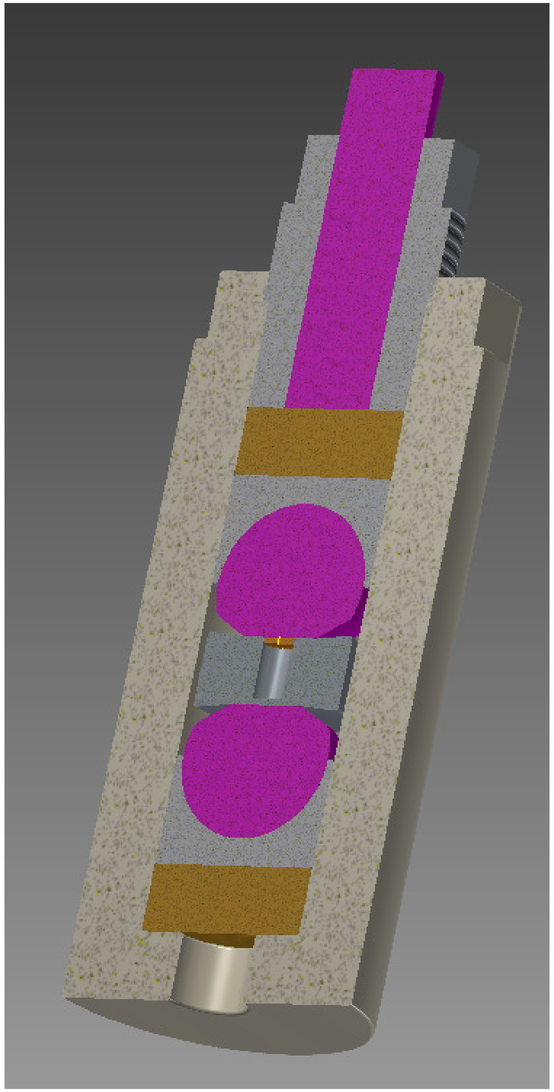

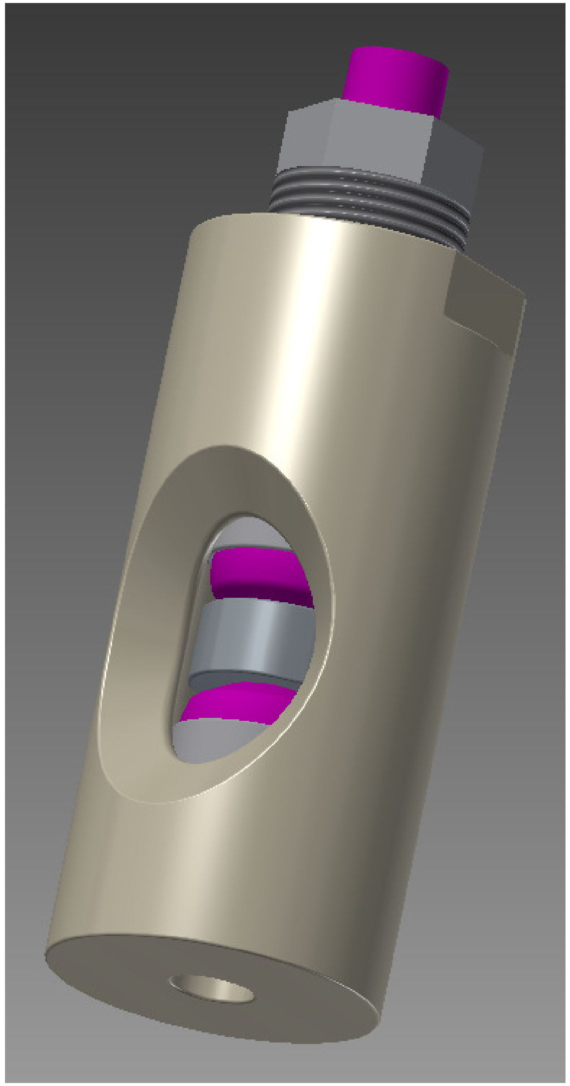

Low-temperature press

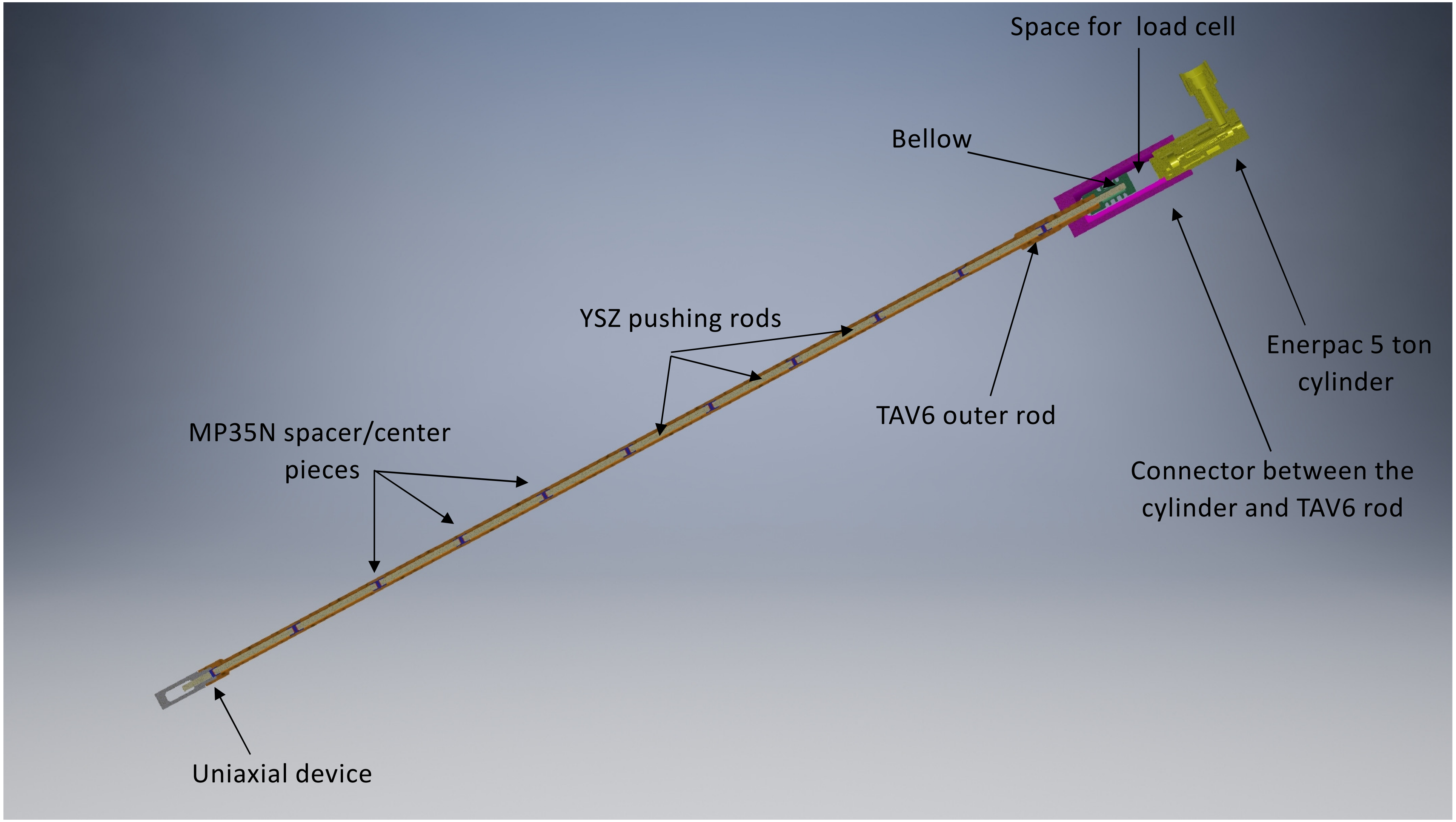

Scientific example: CrAs

CrAs crystal structure

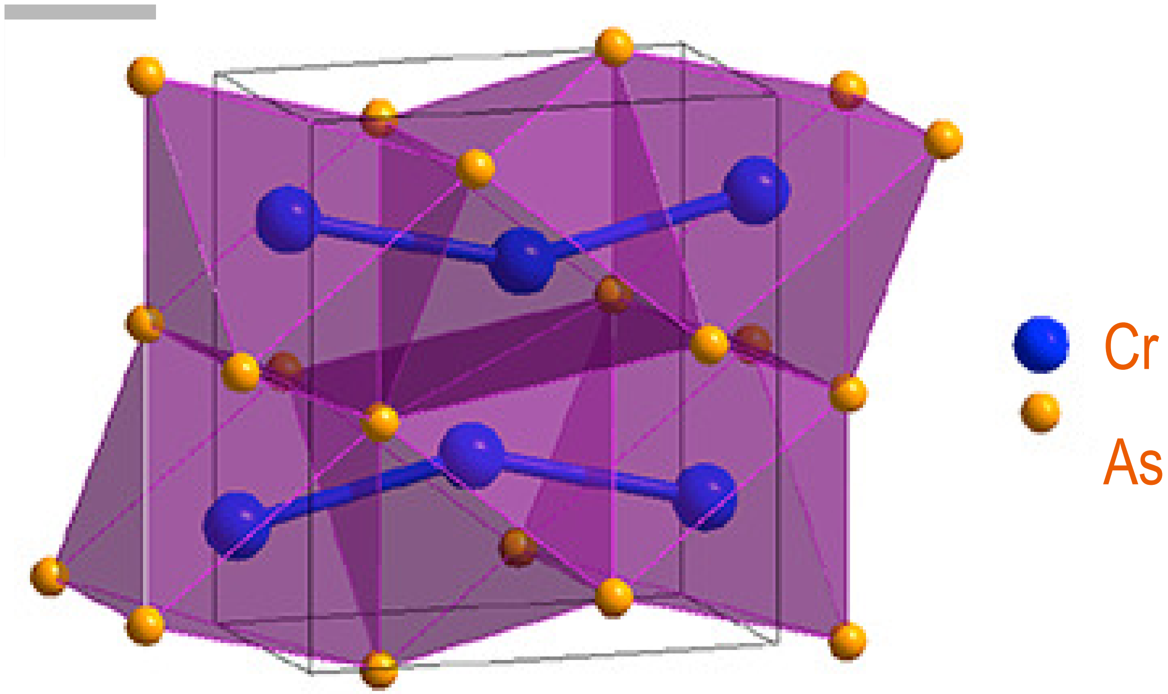

TABLE I. Refined structural and magnetic parameters of CrAs at T = 1.5, 80, and 300 K at ambient pressure; a–c: lattice parameters; x, z: atomic coordinates for site 4c in $Pnma$; B: temperature factor; μ: ordered magnetic moment; ϕ: magnetic phase angle; k_c: component of magnetic propagation vector.

	1.5 K	80 K	300 K
a (Å)	5.6049(3)	5.6068(3)	5.6472(3)
b (Å)	3.5852(2)	3.5846(2)	3.4727(2)
c (Å)	6.1301(5)	6.1304(4)	6.2017(6)
x/Cr (Å)	0.0068(12)	0.0064(12)	0.0060(10)
z/Cr (Å)	0.2034(10)	0.2026(8))	0.2022(10)
B/Cr (Å^2)	0.20(8)	0.32(7)	0.62(8)
x/As (Å)	0.2011(10)	0.2033(14)	0.2021(13)
z/As (Å)	0.5802(12)	0.5792(12)	0.5758(10)
B/As (Å^2)	0.12(5)	0.26(7)	0.51(7)
μ (μ_B)	1.73(2)	1.71(2)	
ϕ (°)	–110(4)	–108(4)	
k_c	0.3562(2)	0.3590(2)	
R_p	5.92	5.83	5.89

Keller *et al.*, PRB 91, 020409(R) (2015)

CrAs magnetic structure

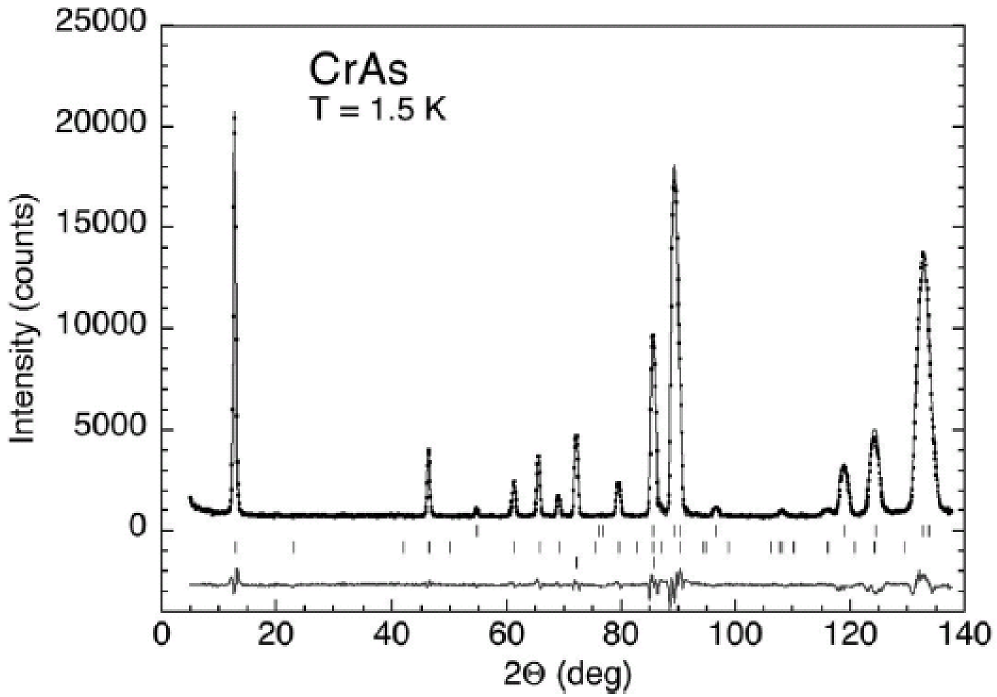

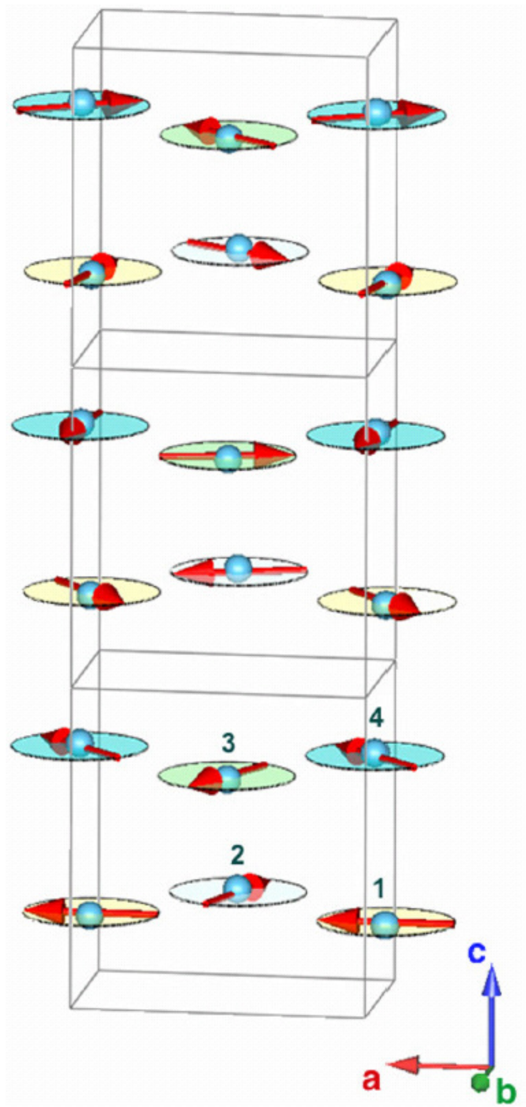

Incommensurate helical magnetic structure. The evolution of the moments for three unit cells along *c*; the four spirals are marked in individual colors. The propagation vector k_c=0.3562(2) φ is defined as the angle between the moments of Cr atoms 1 and 2 (or 3 and 4). Ordering temperature T_N=265K.

Keller *et al.*, PRB 91, 020409(R) (2015)

Pressure induced superconductivity in CrAs

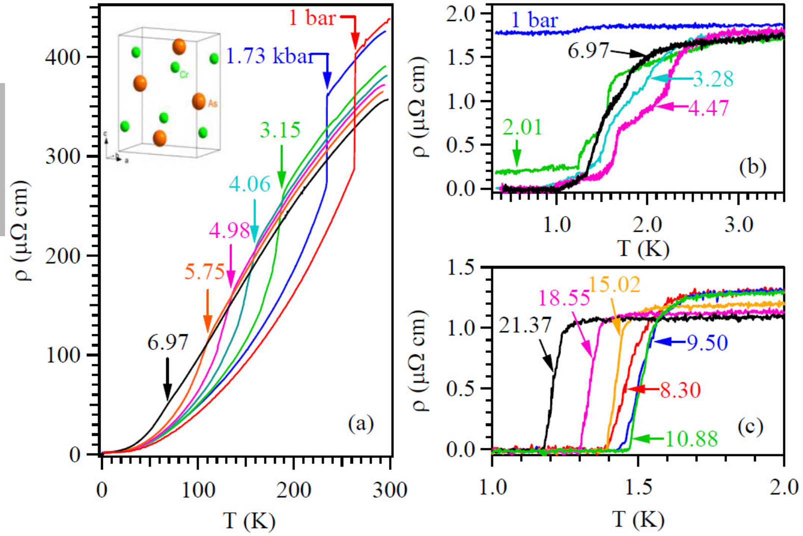

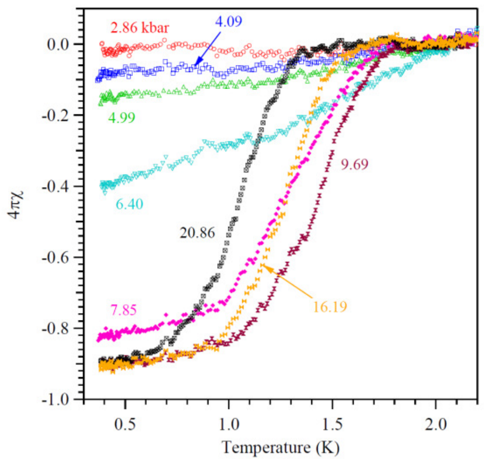

Wu *et al*., Nat. Comm. **5**, 5508 (2014)

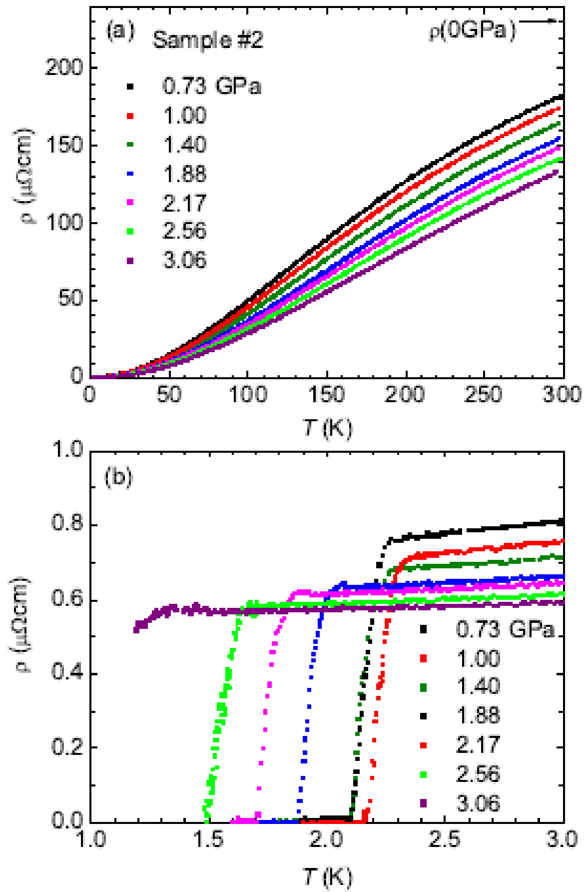

Kotegawa *et al*., PRL **114**, 117007 (2015)

Proposed phase diagrams

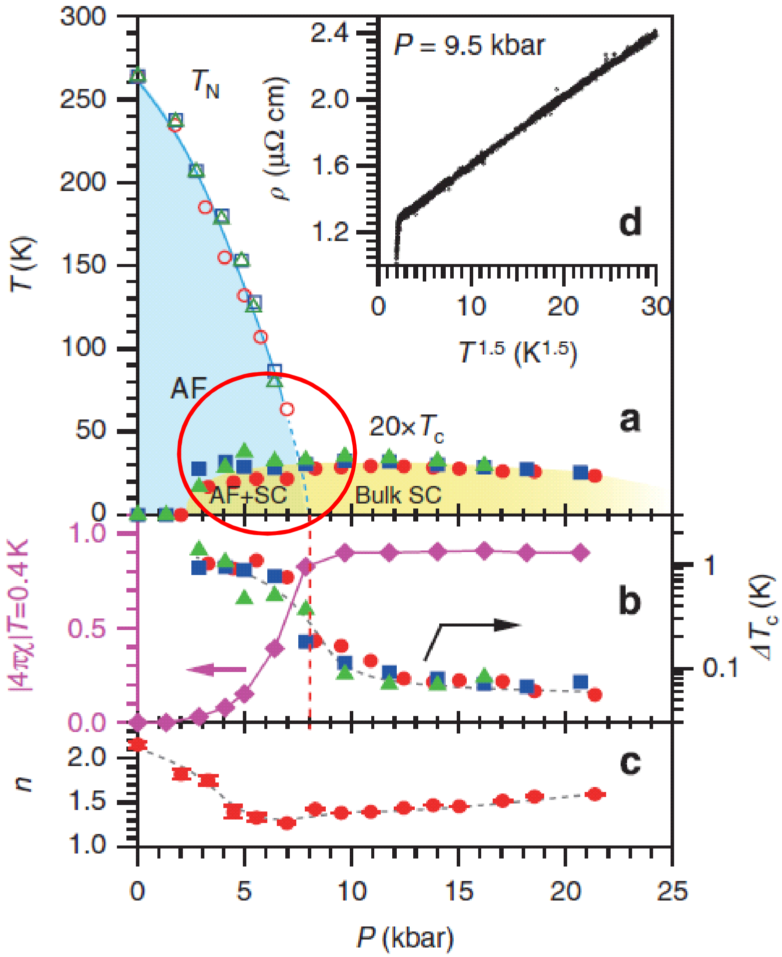

Wu *et al.*, Nat. Comm. **5**, 5508 (2014)

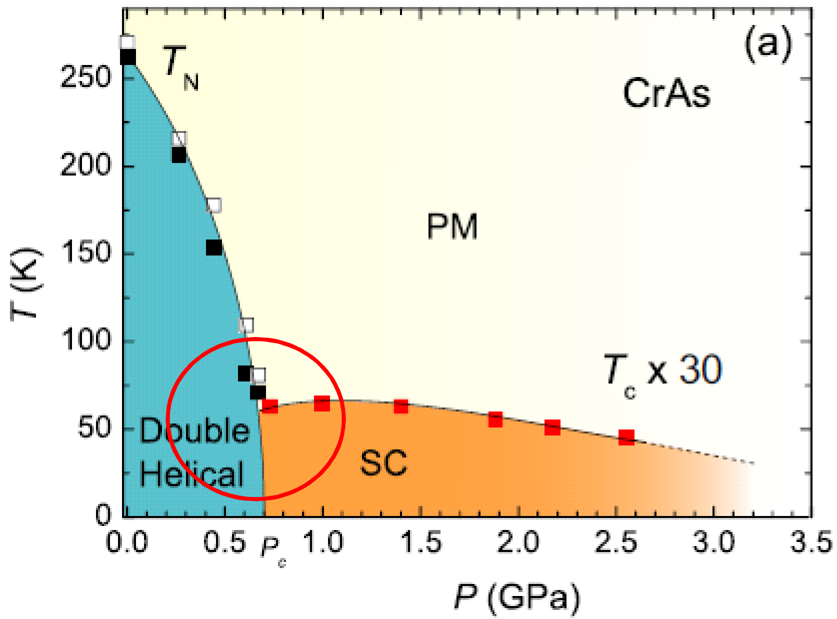

Kotegawa *et al.*, PRL **114**, 117007 (2015)

Unanswered questions

1. **How magnetism is suppressed?**

2. **How occurs the superconductivity?**

3. **Is there any coexistence/interplay between these two phenomena?**

Helical magnetic order

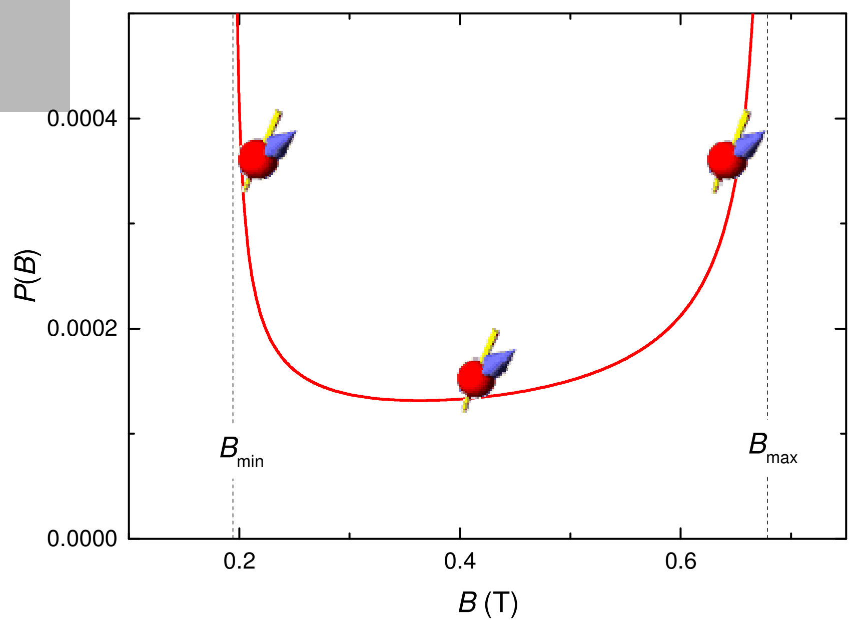

$$P(B) = \frac{2}{\pi} \frac{B}{\sqrt{(B^2 - B_{min}^2)(B_{max}^2 - B^2)}}$$

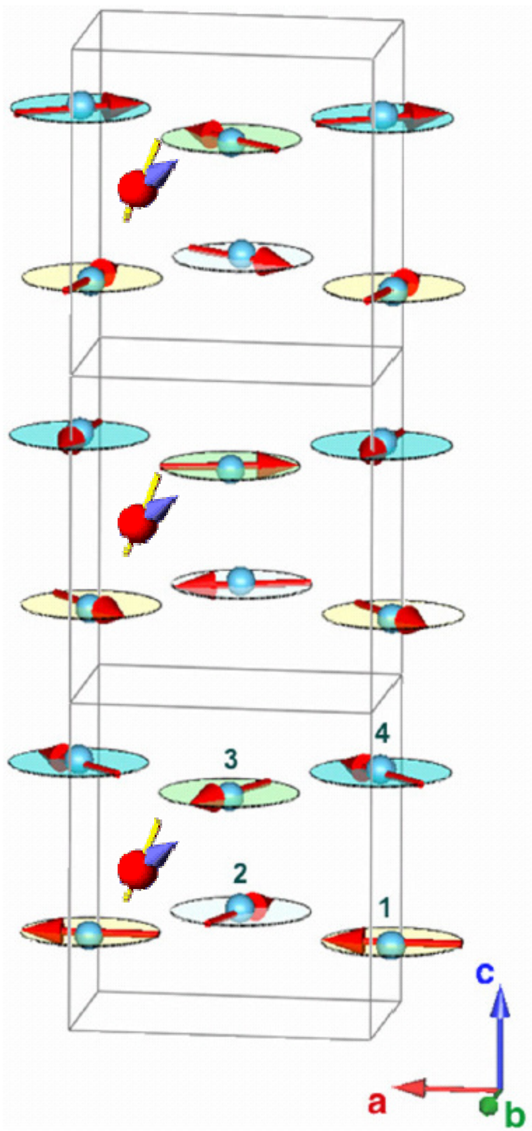

Helical magnetic order

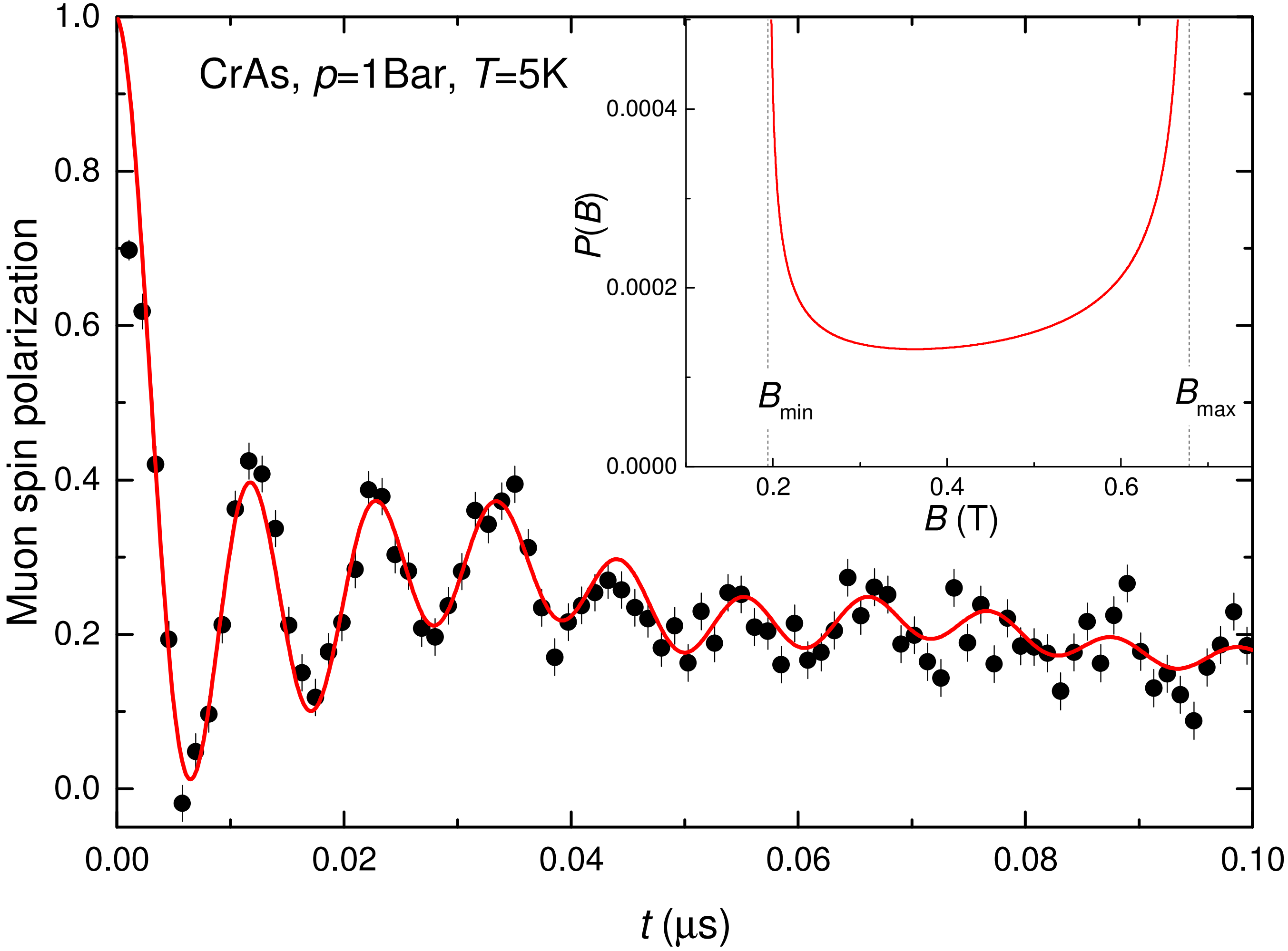

Confirmation of helical type of magnetic order in CrAs

B_{min} and B_{max} as a function of p

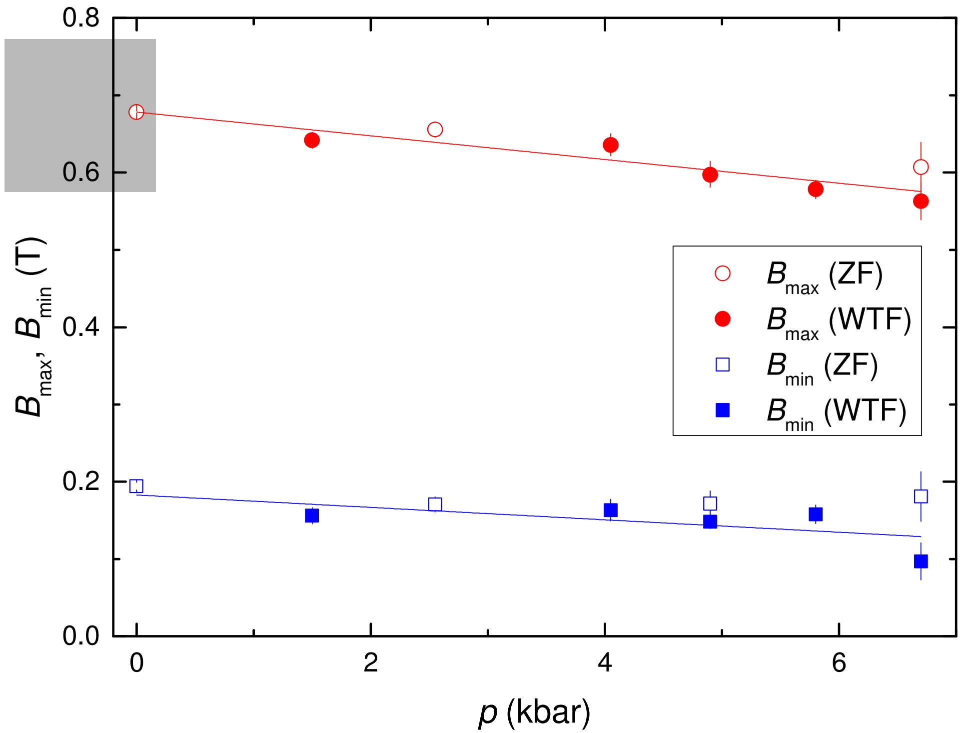

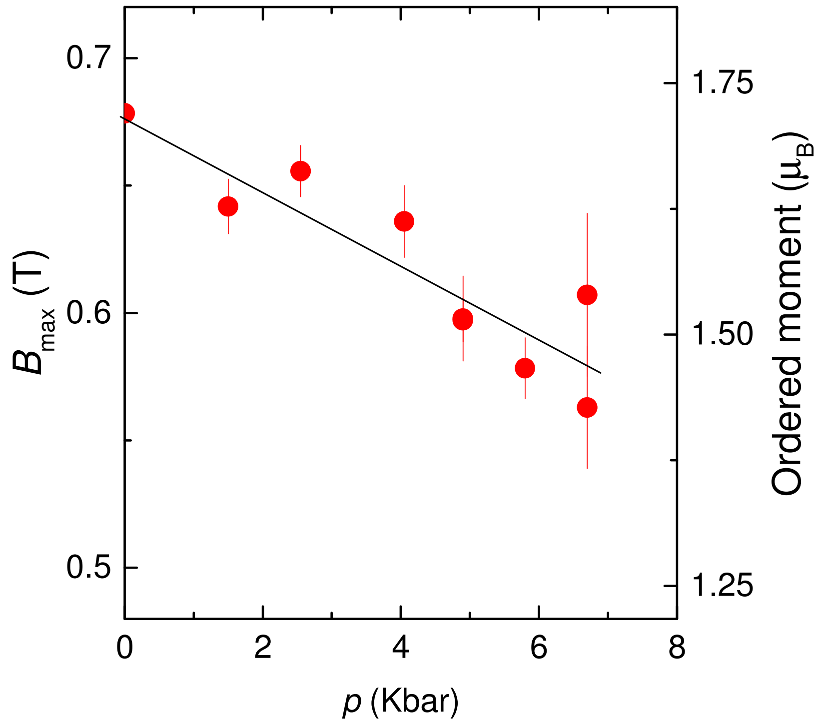

The internal field on the muon stopping site is proportional to the ordered moment. Increase of pressure from 1bar to 7Kbar leads to decrease of Cr moments from 1.73μ_B to 1.47μ_B

Weak transverse field (WTF)

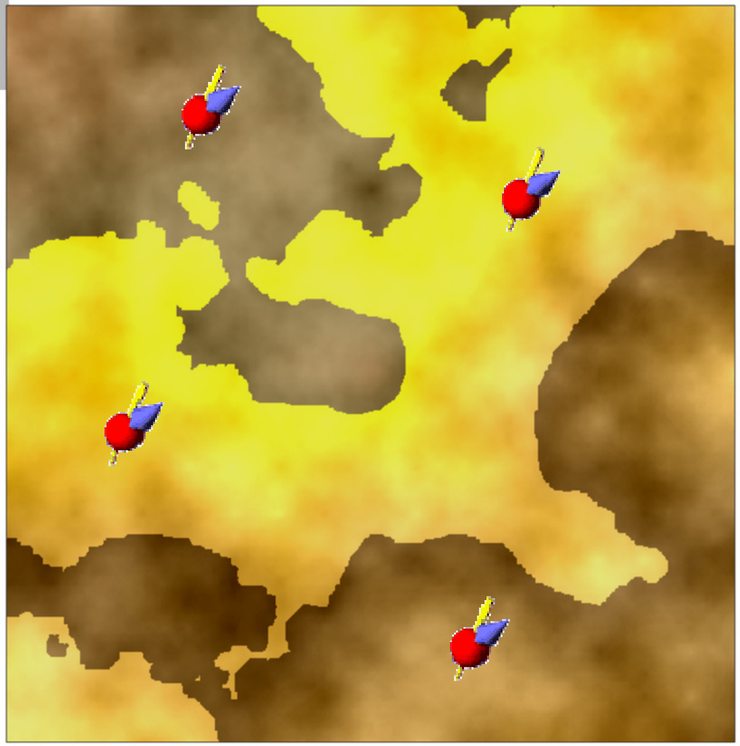

- Local field at the muon stopping position is the vector sum of the "internal" (B_{int}) and the "applied" (B_{app}) one
  - $B_{\mu}=B_{int}+B_{app}$

- In a case $B_{int}>>B_{app}$ (weak field regime)
- $B_{\mu}=B_{int}$ in the magnetically ordered parts
- $B_{\mu}=B_{app}$ in paramagnetic parts

PAUL SCHERRER INSTITUT PSI

WTF experiments

WTF 3mT

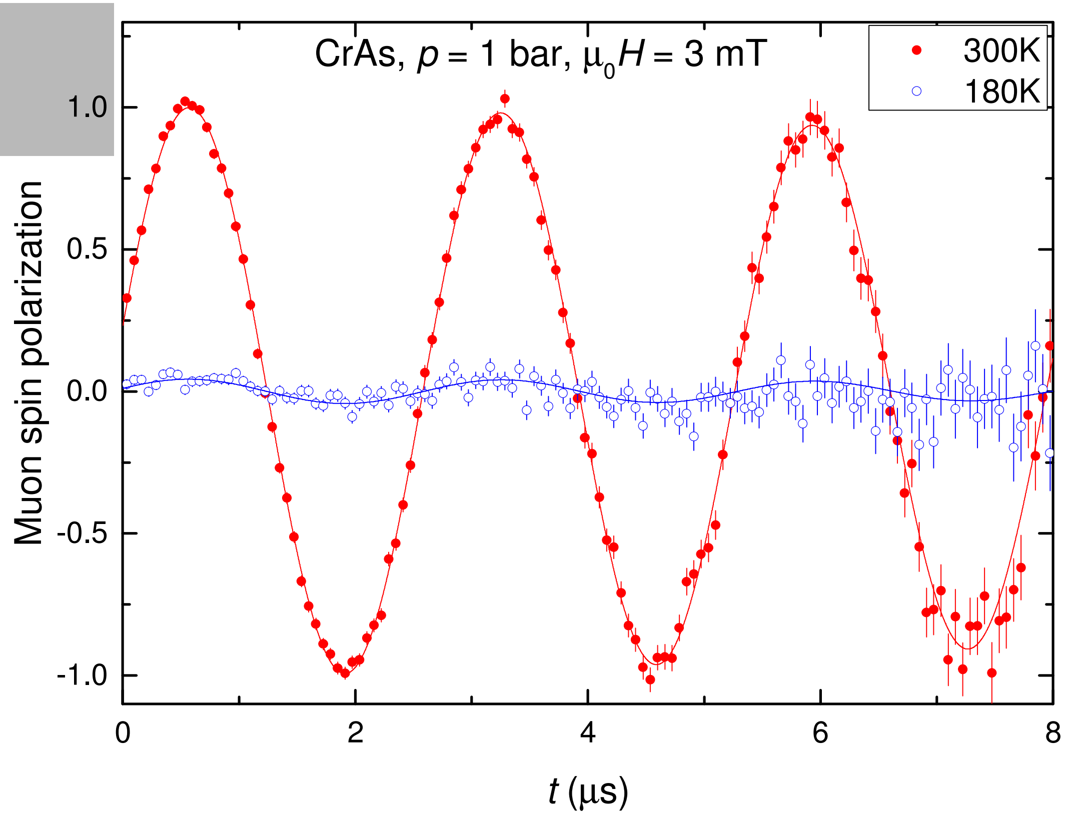

ZF

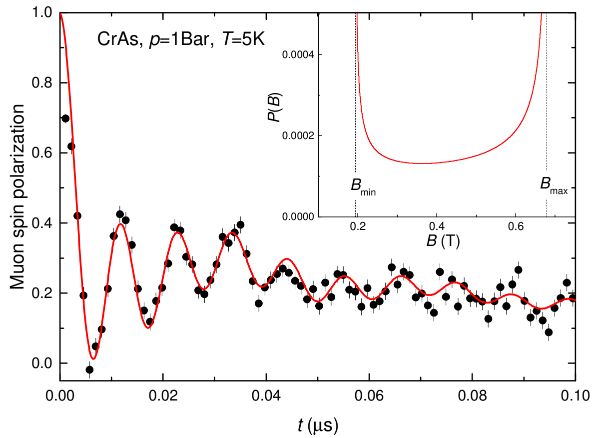

WTF experiments

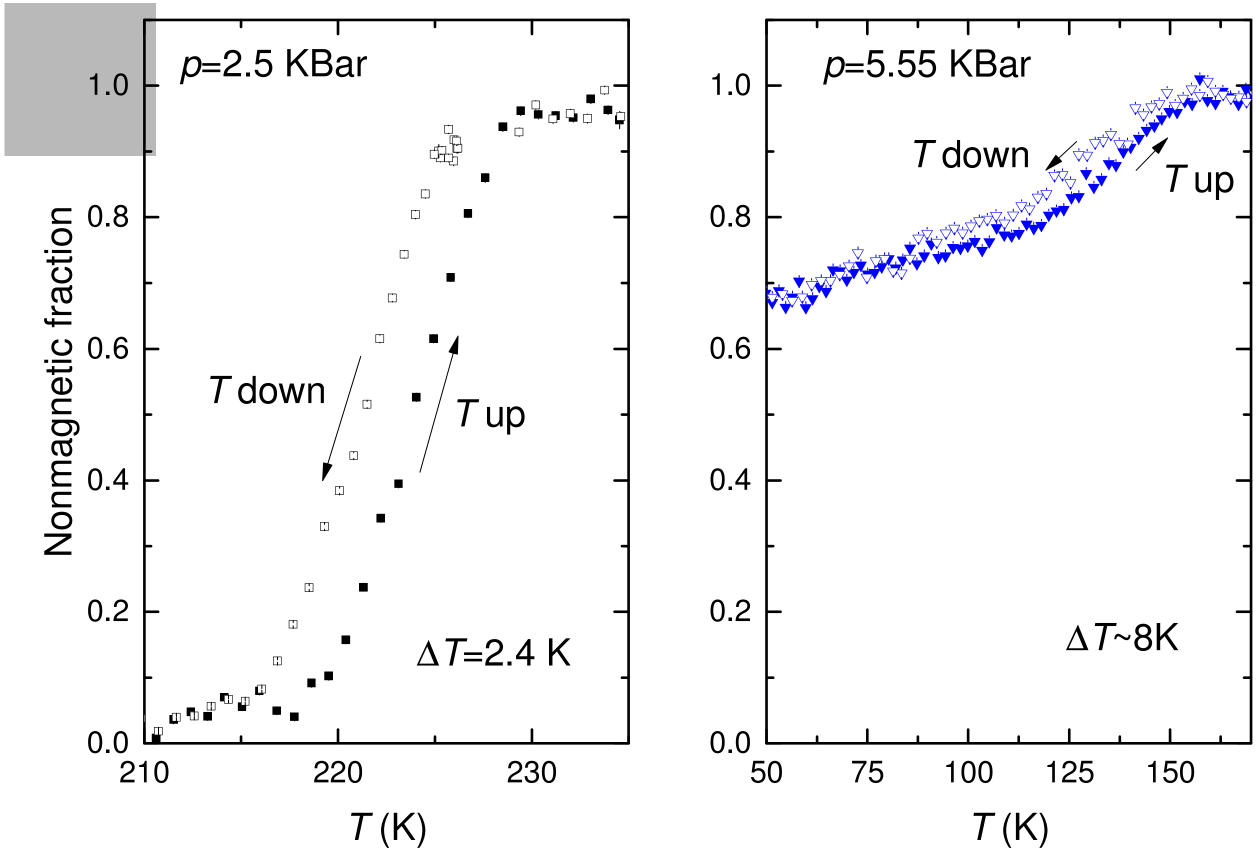

- The magnetic transition is first order like
- Transition temperature decreases with increasing pressure
- Magnetic volume fraction decreases with pressure increase

Summary of WTF experiments

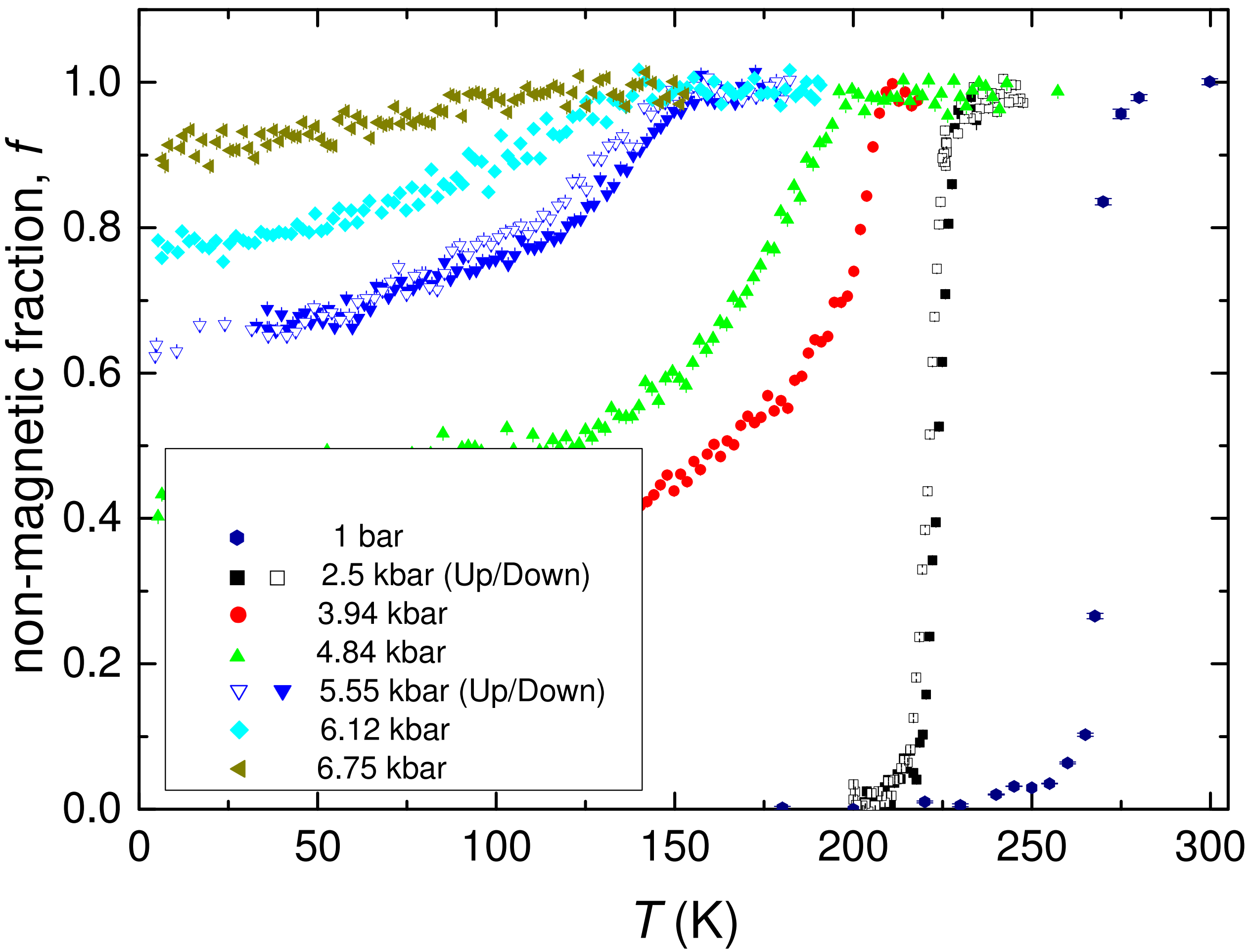

No magnetism above p~7 Kbar!

Magnetic response of CrAs

T_N

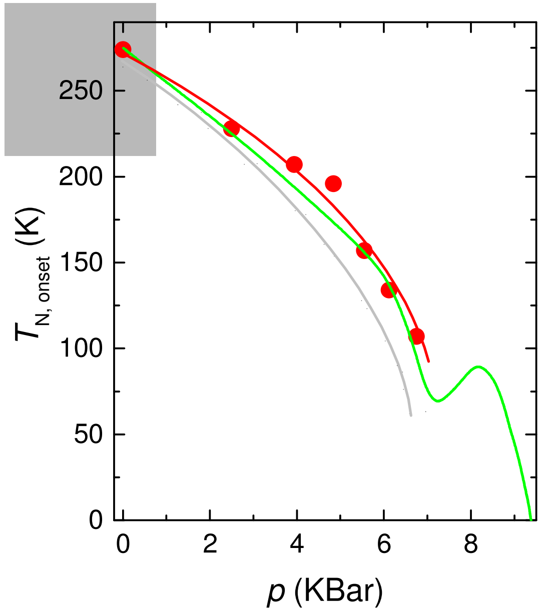

Nonmagnetic fraction

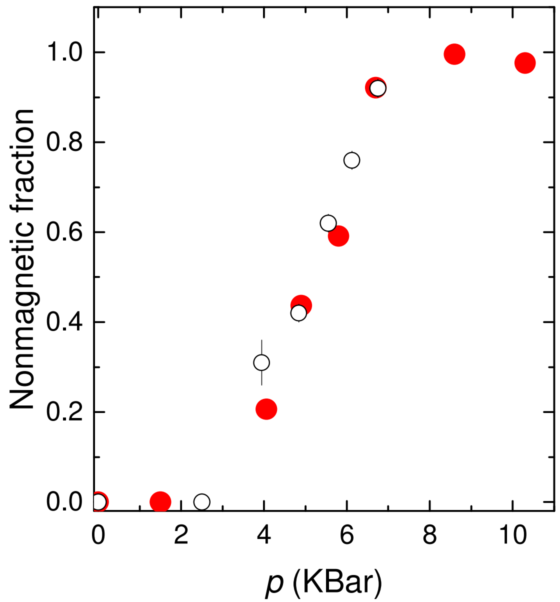

Ordered moment

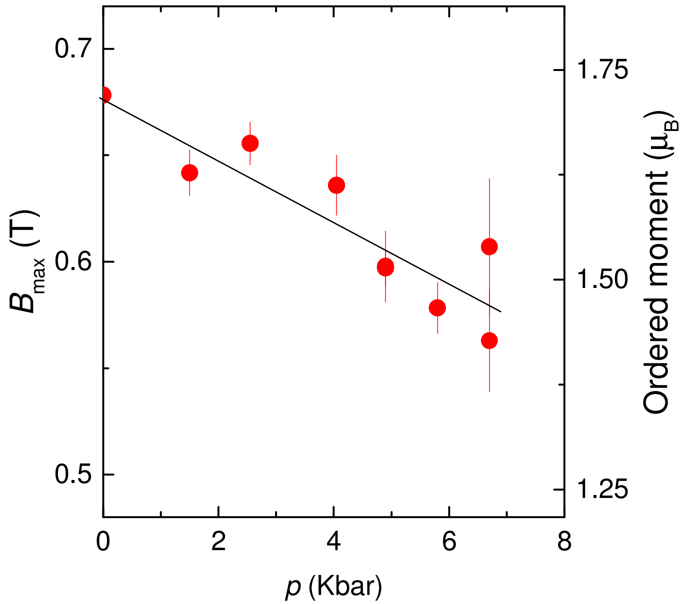

Wu *et al.*, Nat. Comm. **5**, 5508 (2014)

Kotegawa *et al.*, PRL **114**, 117007 (2015)

Shen *et al.*, arxiv:1409.6615

Comparison with neutron data

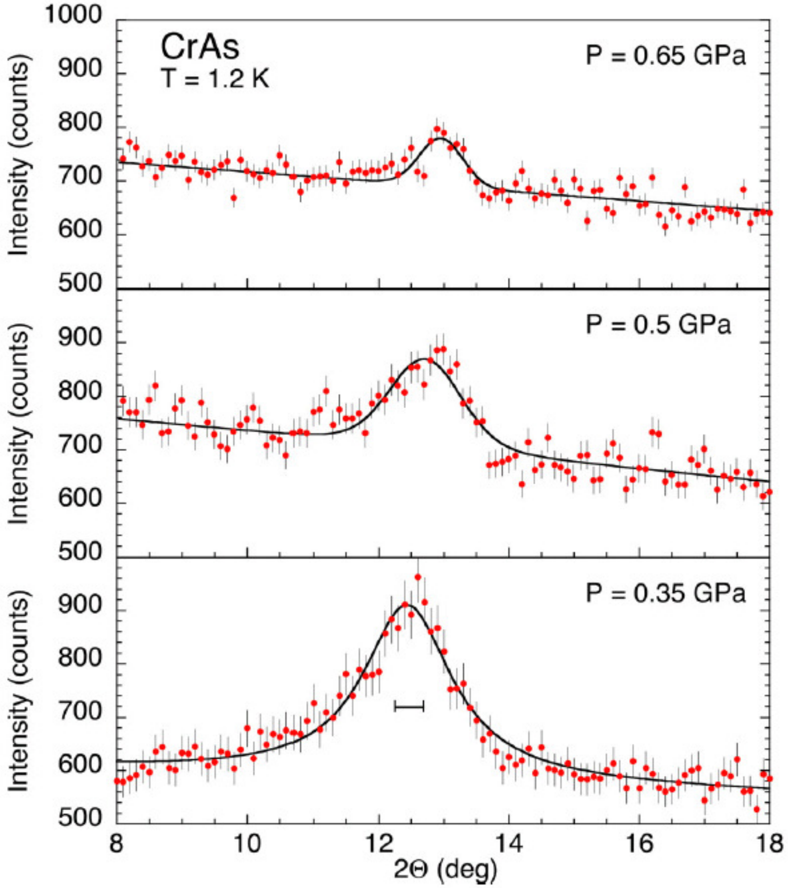

FIG. 4. (Color online) Pressure dependence of the first magnetic satellite ($00 \pm k_c$) for the pressures $P = 0.35$, 0.5, and 0.65 GPa. A convolution of Lorentzian and Gaussian peak shape functions was used for the profile fits.

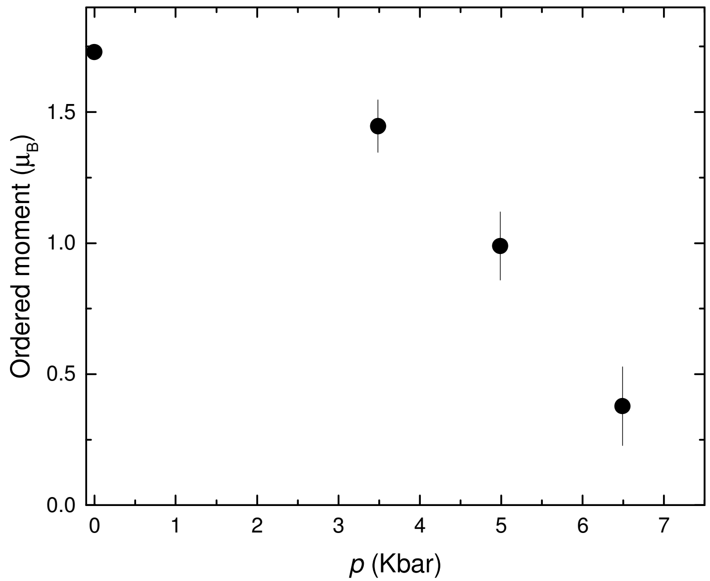

Keller *et al.*, PRB 91, 020409(R) (2015)

Comparison with neutron data

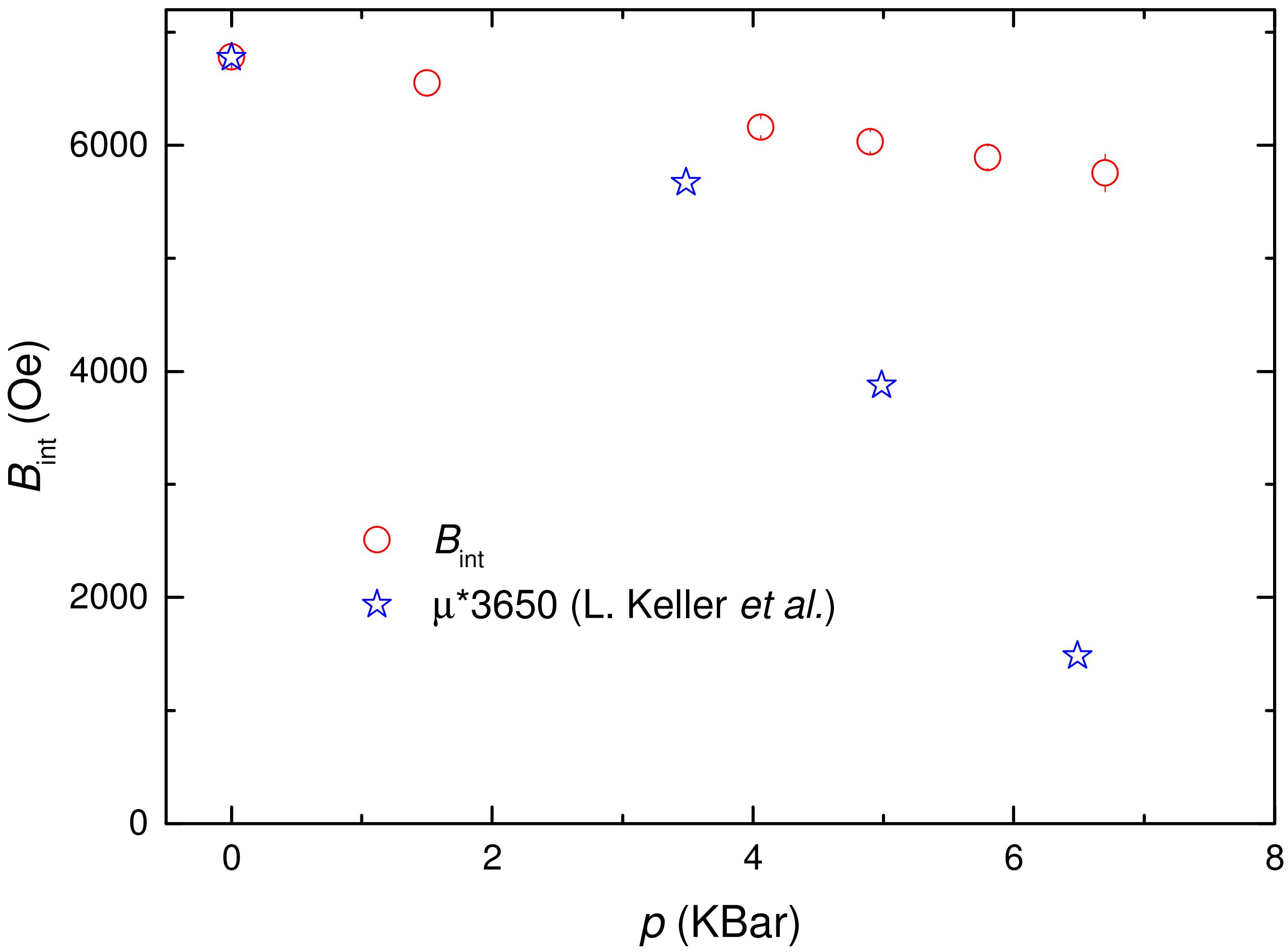

Comparison with neutron data

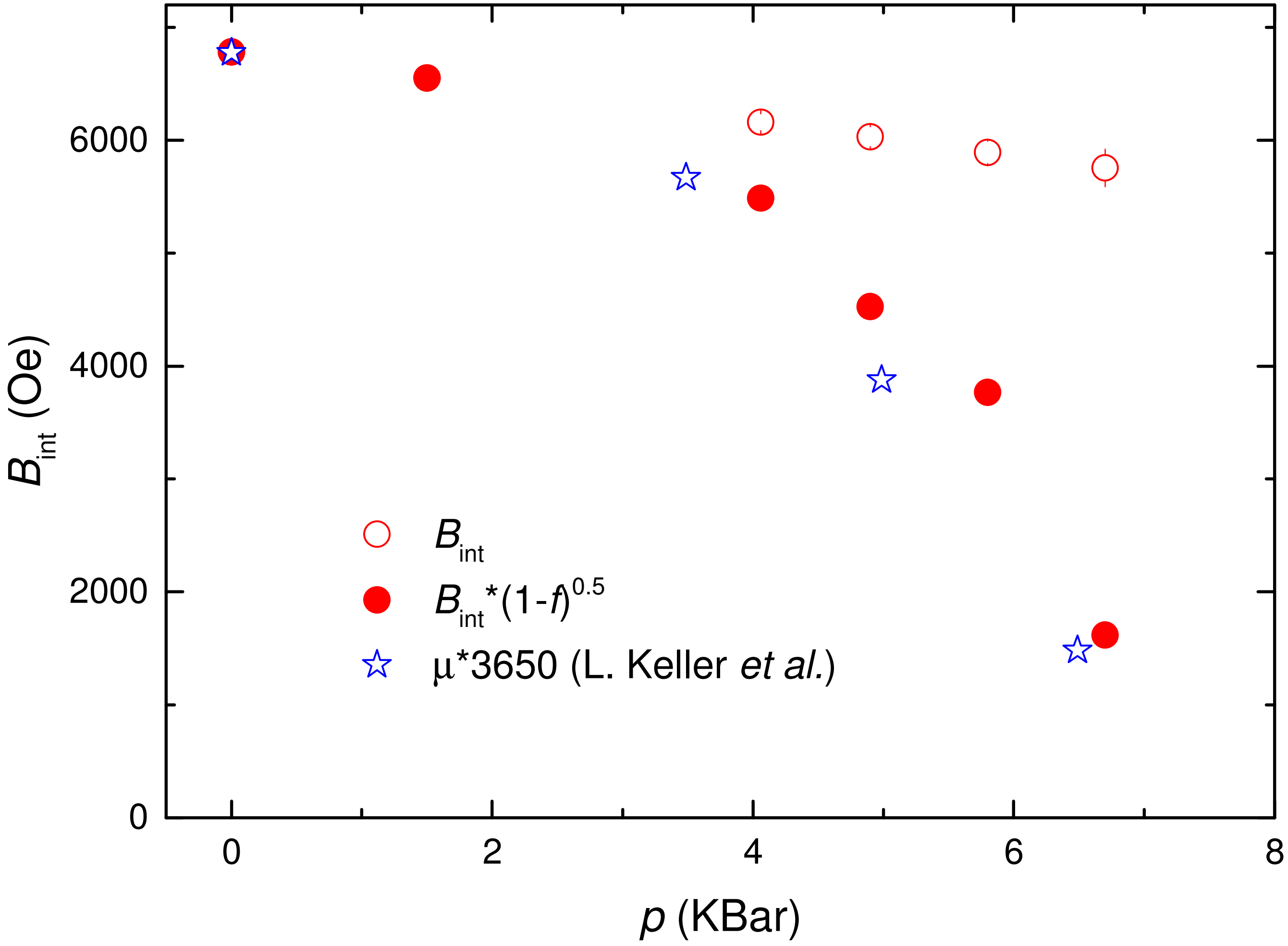

Field Distribution in a Type II S.C.

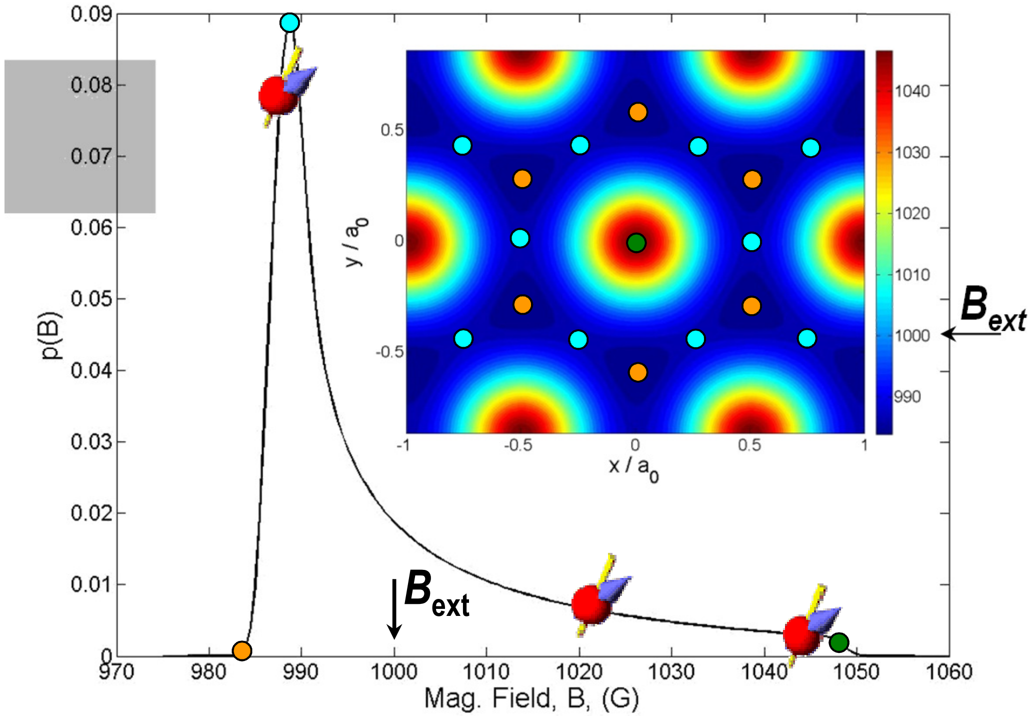

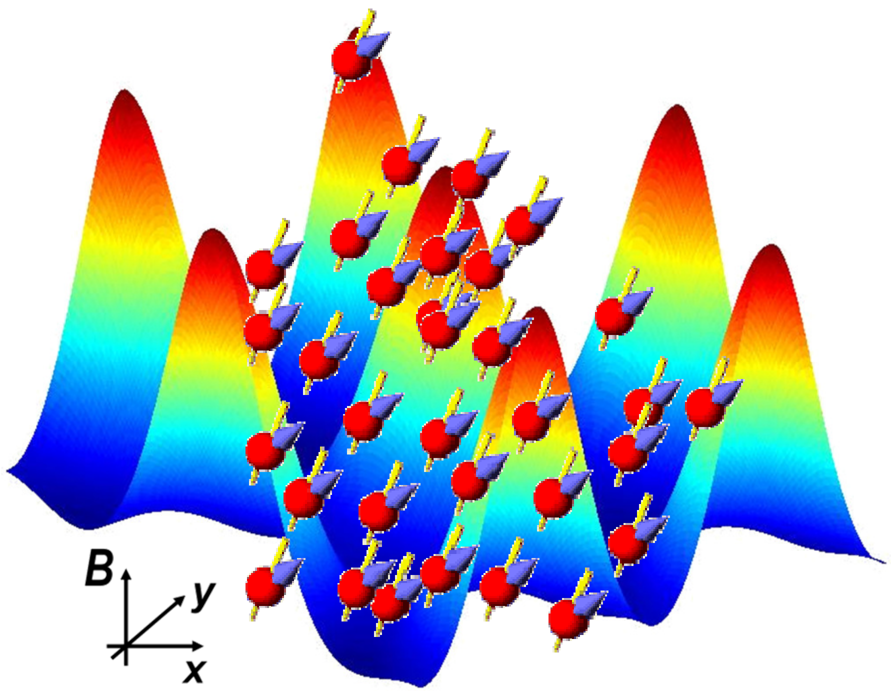

Since the muon is a local probe, the μSR relaxation function is given by the weighted sum of all oscillations:

$$G(t) = \int f(\mathbf{B}_\mu) \cos(\gamma_\mu B_\mu t) d\mathbf{B}_\mu$$

Extract Information from the μSR data

$$G(t) = \underbrace{\exp(-\frac{1}{2}\sigma^2 t^2)}_{\text{depolarization}} \times \underbrace{\cos(\gamma_\mu \langle B_\mu^z \rangle t)}_{\text{oscillations}}$$

where: $\sigma^2 = \gamma_\mu^2 \langle \Delta B_\mu^{z\,2} \rangle$

Pümpin et al., Phys. Rev. B ***42****, 8019 (1990)*

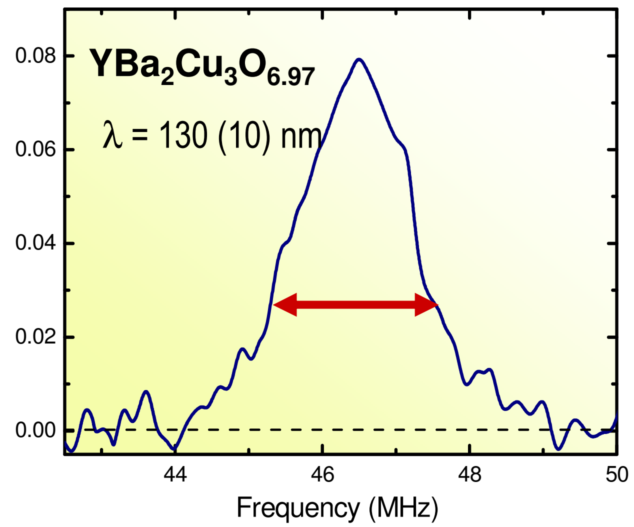

Ginzburg-Landau model

$$\langle \Delta B_z^2 \rangle = 0.00371 \frac{\phi_0^2}{\lambda^4}$$

A μSR measurement of the second moment of the field distribution allows to determine the London penetration depth λ.

London model

$$\lambda = \sqrt{\frac{m}{\mu_0 e^2 n_s}}$$

$$\Rightarrow \quad \sigma \propto \frac{1}{\lambda^2} \propto \frac{\mu_0 e^2}{m} n_s$$

The damping of a TF-μSR spectrum is proportional to the super fluid density n_s (number of Cooper pairs).

After H. Luetkens (Sunday 16 Aug 2015)

TF 30mT

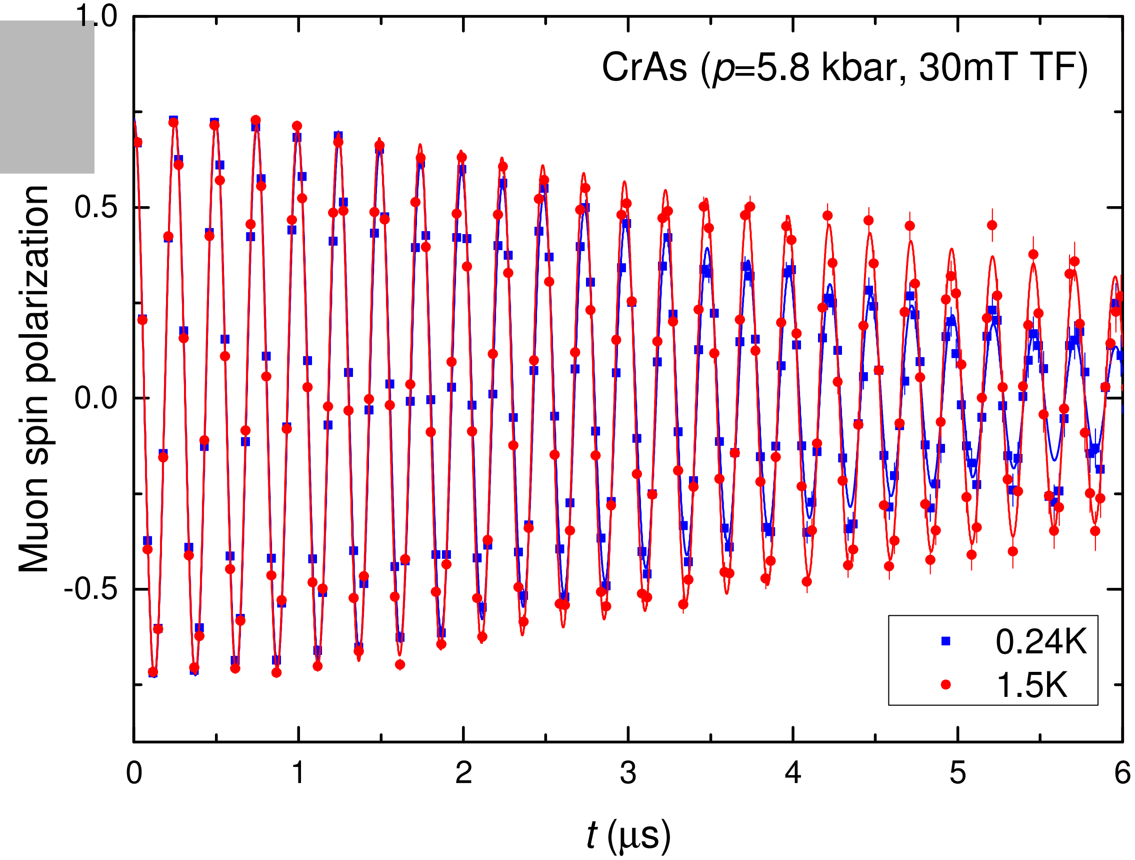

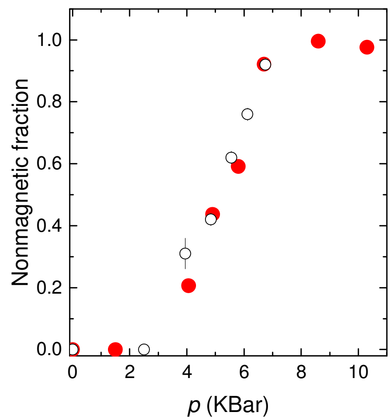

Appr. 20% of the sample remains in the magnetic state

TF 30mT

Superfluid density

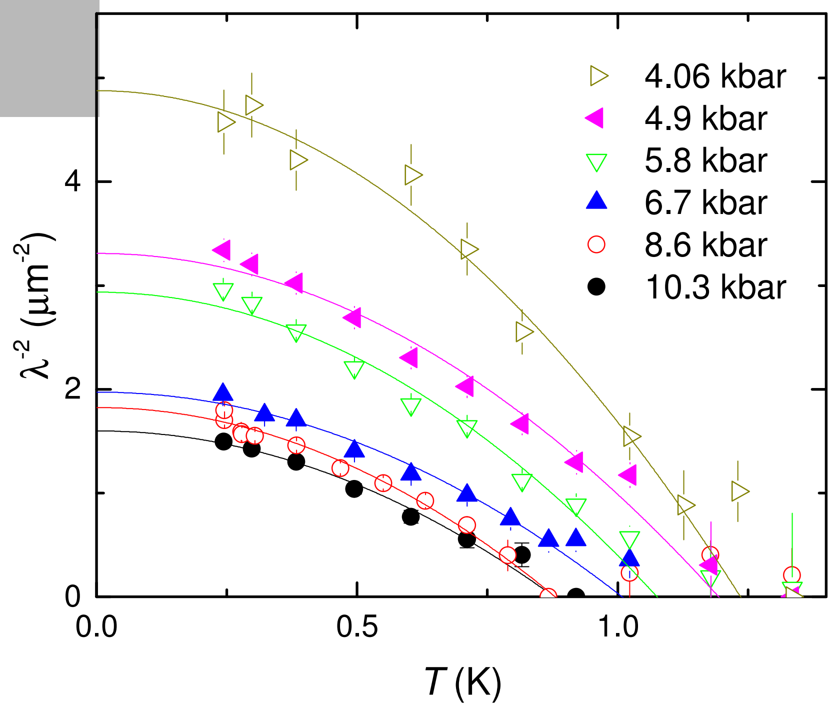

Diamagnetic shift

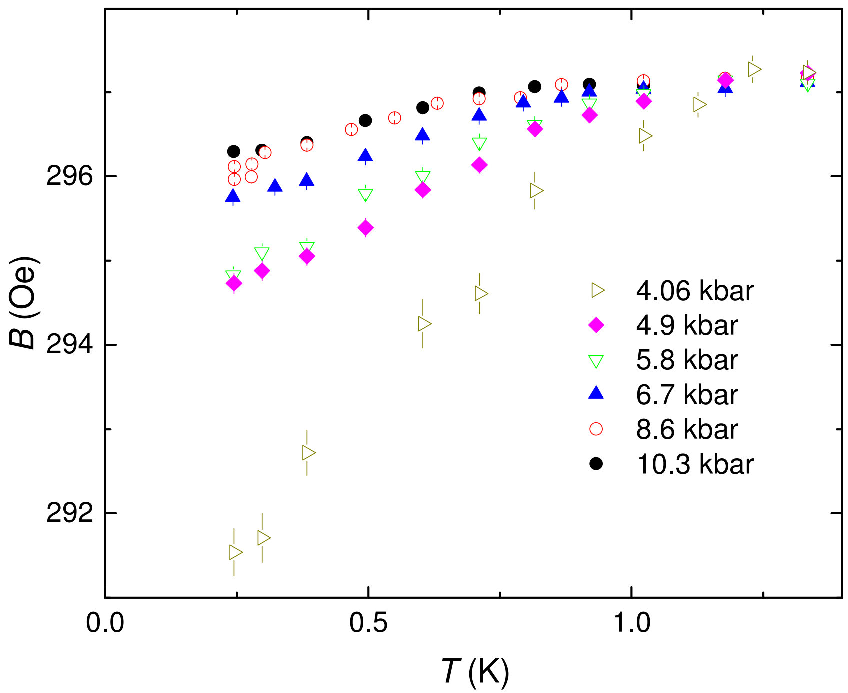

Phase coexistence in CrAs

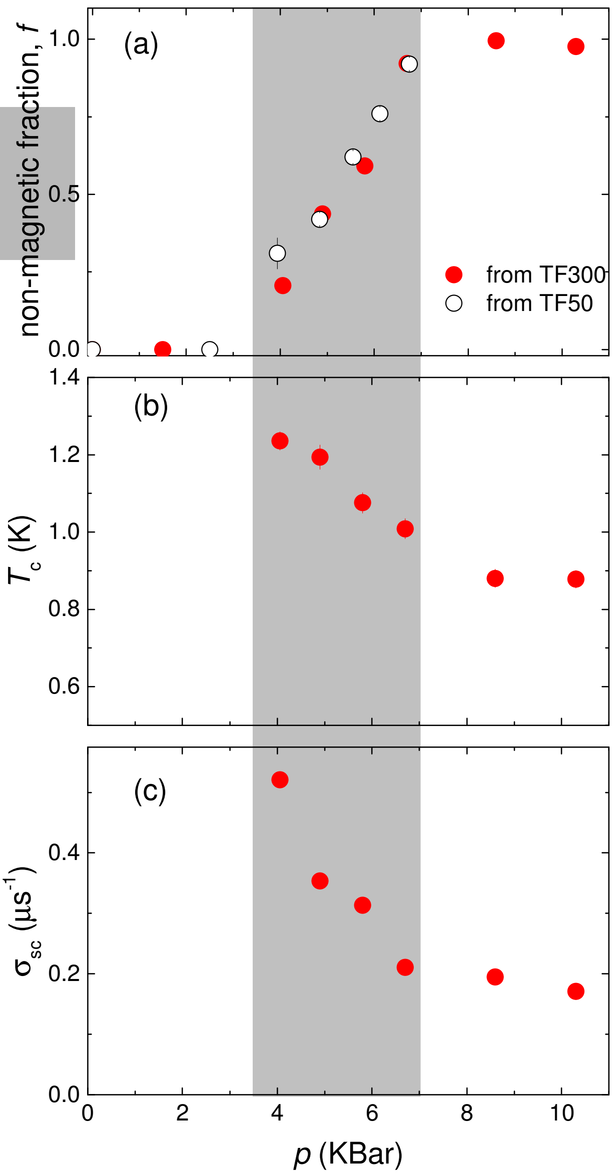

- CrAs is purely magnetic up to p~3.5kbar
- For 3.5<p<7kbar magnetic and superconducting responses are detected in a set of ZF, wTF, and TF experiments. CrAs is phase separated into volumes where long range magnetic order sets at T_N and into non-magnetic volumes becoming superconducting below T_c.
- Above 7kbar and above T_c the sample is purely in the paramagnetic state. Bulk superconductivity sets below T_c.

Self-doping effect

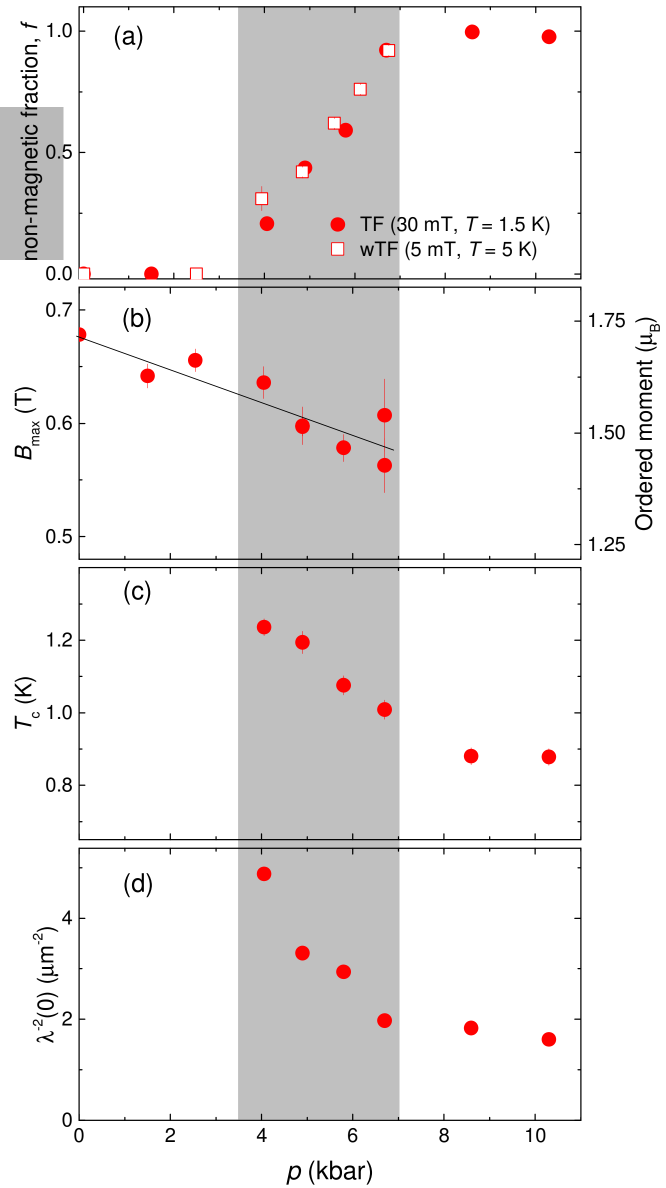

- Besides the competition for the volume, there is no evidence for a competition between the magnetic and superconducting order parameter in CrAs:
  1. The ordered magnetic moment stays almost constant, by changing less than 15%.
  2. T_N, evolves smoothly with pressure without showing any pronounced features at p~3.5-4kbar

– The maximum value of $\rho_s \sim \lambda^{-2} \sim n_s/m^*$ is observed at the low pressure side of the phase separated region -- in the region where the non-magnetic volume fraction *f* is the smallest.

– By neglecting the pressure effect on m*,

$$\rho_s \sim n_s$$

carriers from the 'less conductive' magnetically ordered parts of the sample can be supplied to the 'more conductive' non-magnetic parts -- self doping effect!

Conventional vs. unconventional superconductivity

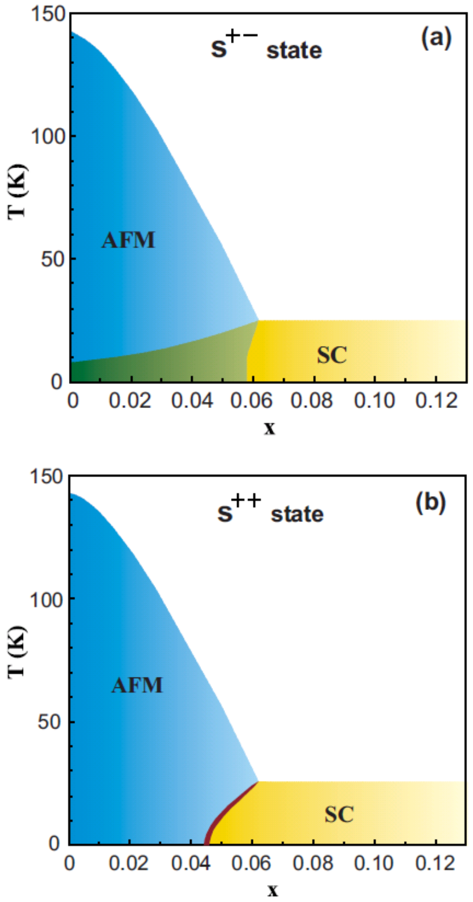

FIG. 1. (Color online) Phase diagrams of $Ba(Fe_{1-x}Co_x)_2As_2$ for a superconducting (a) s^{+-} state and an (b) s^{++} state, obtained by numerically solving the gap equations. The green region denotes homogeneous, microscopic coexistence, whereas the dark red region denotes heterogeneous, macroscopic coexistence. The band-structure parameters are discussed in Sec. IV B.

Fernandes et al., PRB 82, 014521 (2010)

- The relative phase difference (θ) of the superconducting order parameter between different parts of Fermi surface or Fermi surface sheets may lead either to stabilization of microscopic coexistence of the magnetic and superconducting phases or drive both to repel each others:

  - $F_J \propto M^2 |\Delta_1| |\Delta_2| \cos\vartheta$

– For conventional superconductivity Θ=0, F_J increases making two phases unlikely to coexist

– For $\Theta=\pi$, F_J is negative. Both the superconducting and the magnetic phases tend to coexist.

Correlation between T_c and λ^{-2}

Cuprates

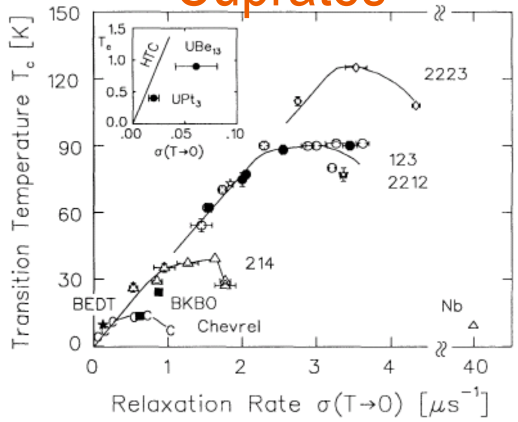

$\lambda^{-2} \propto T_c$

Uemura *et al.* PRL **66**, 2665 (1991)

Molecular s.c.

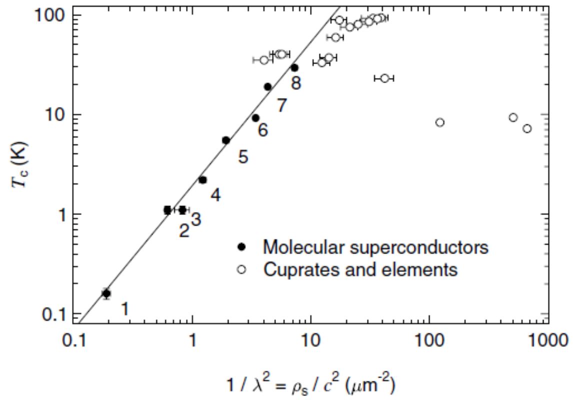

$\lambda^{-2} \propto T_c^{2/3}$

Pratt and Blundell PRL **94**, 097006 (2005)

Fe-based

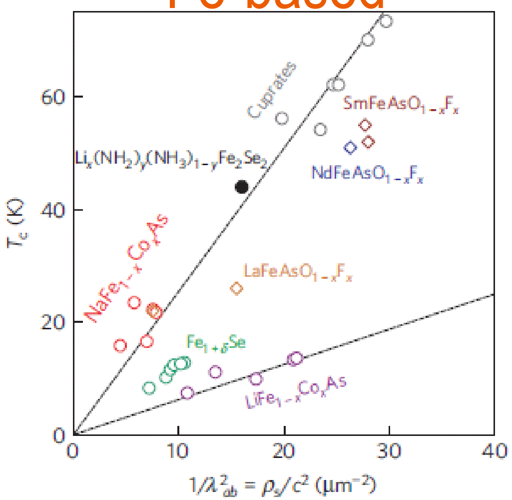

$\lambda^{-2} \propto T_c$

Burrard-Lucas *et al.* Nature Mat. **12** 15 (2013)

BCS s.c.

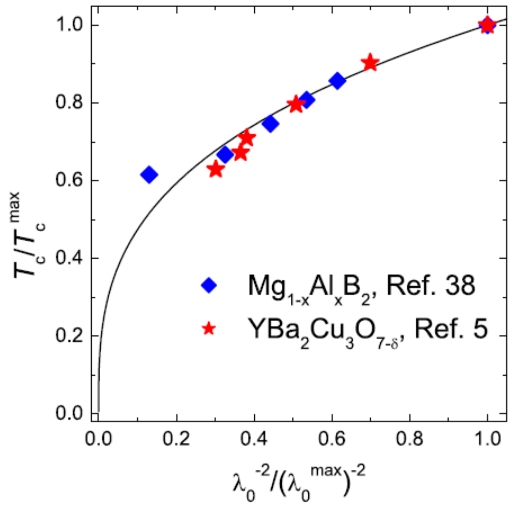

$\lambda^{-2} \propto T_c^{3.1}$

Khasanov et al. PRB **77**, 064506 (2008)

Correlation between T_c and λ^{-2}

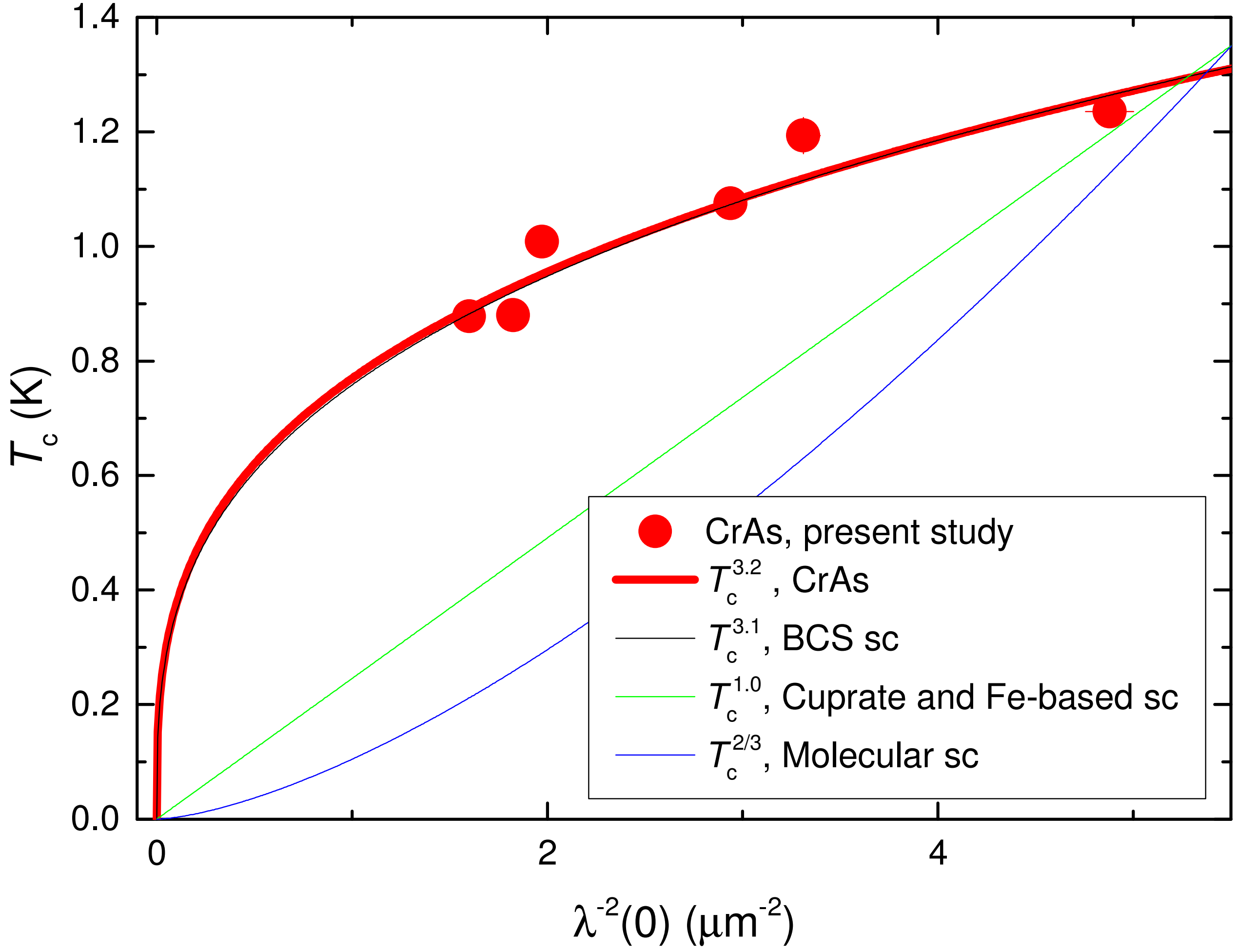

Conclusions

- The bulk magnetism exists up to p~3.5kbar, while the purely non-magnetic state develops for pressures above ~7kbar.
- In the intermediate pressure region ($3.5<p<7$kbar) the magnetic phase volume decreases continuously and superconductivity develops in parts of the sample remaining non-magnetic down to the lowest temperatures.
- Both, the superconducting transition temperature T_c and the zero-temperature superfluid density $\rho_s(0)$ decrease with increasing pressure in the intermediate pressure region and saturate for p exceeding 7kbar i.e. in the region where magnetism is completely suppressed.
- The pressure-induced transition of CrAs from a magnetic to a superconducting state is characterized by a separation in macroscopic size magnetic and superconducting volumes. The less conductive magnetic phase provides additional carriers (doping) to the superconducting parts of CrAs.
- The superfluid density was found to scale with T_c as $T_c^{3.2}$, which, together with the clear phase separation between magnetism and superconductivity, points towards a conventional mechanism of the Cooper-pairing in CrAs.

Thanks

- M. Elender, A. Maisuradze, Z. Guguchai, G. Simutis, Z. Shermadini, T. Goko, F. Knechet, H. Luetkens, A. Amato, E. Morenzoni
  - Laboratory for Muon Spin Spectroscopy, Paul Scherrer Institute

- D. Andreica

Faculty of Physics, Babes-Bolyai University, Cluj-Napoca, Romania

- S. Klotz

IMPMC, CNRS UMR 7590, Sorbonne Université, Paris, France

- K Kamenev

Centre for Science at Extreme Conditions and School of Engineering, The University of Edinburgh, Scotland, UK